The influence of light on nitrogen cycling and the primary nitrite maximum in a seasonally stratified sea

Katherine RM Mackey[1,2,3], Laura Bristow[4], David R Parks[5], Mark A Altabet[4], Anton F Post[6], and Adina Paytan[3]

[1] Corresponding author, kmackey@stanford.edu, 301.356.4041
[2] Department of Civil and Environmental Engineering, Stanford University, Stanford, CA 94305
[3] Institute of Marine Sciences, University of California Santa Cruz, Santa Cruz, CA 95064
[4] School for Marine Science and Technology, University of Massachusetts Dartmouth, New Bedford, MA 02744
[5] Stanford Shared FACS Facility, Stanford University School of Medicine, Stanford, CA 94305
[6] The Josephine Bay Paul Center for Comparative Molecular Biology and Evolution, Marine Biological Laboratory, Woods Hole, MA 02543

Key words:
Nitrogen cycle, primary nitrite maximum, nitrification, light, mixing and stratification, spring bloom

Regional index terms:
Middle East, Red Sea, Gulf of Aqaba, open ocean

Acknowledgements

We thank our colleagues at the Interuniversity Institute for Marine Science in Eilat, Israel for assisting in data collection and providing laboratory space and equipment during the study. C. Danford and R. Foster assisted with sampling, D. Iluz provided PAR data, S. Monismith provided mixing rates, and T. Rivlin and M. Chernichovsky assisted with sampling and nutrient analyses. Monthly monitoring data was accessed from http://www.iui-eilat.ac.il/NMP. This research was supported under the North Atlantic Treaty Organization (NATO) Science for Peace Grant SfP 982161 to AP and AFP, a grant from the Koret Foundation to AP, a National Science Foundation Biological Oceanography grant to AP, the Israel Science Foundation grant 135/05 to AFP, and research grant 8330-06 from the Geological Society of America to KRMM. KRMM was supported through the National Science Foundation (NSF) Graduate Research Fellowship Program and the Department of Energy (DOE) Global Change Education Program.

Abstract

In the seasonally stratified Gulf of Aqaba Red Sea, both NO_2^- release by phytoplankton and NH_4^+ oxidation by nitrifying microbes contributed to the formation of a primary nitrite maximum (PNM) over different seasons and depths in the water column. In the winter and during the days immediately following spring stratification, NO_2^- formation was strongly correlated (R^2=0.99) with decreasing irradiance and chlorophyll, suggesting that incomplete NO_3^- reduction by light limited phytoplankton was a major source of NO_2^-. However, as stratification progressed, NO_2^- continued to be generated below the euphotic depth by microbial NH_4^+ oxidation, likely due to differential photoinhibition of NH_4^+ and NO_2^- oxidizing populations. Natural abundance stable nitrogen isotope analyses revealed a decoupling of the $\delta^{15}N$ and $\delta^{18}O$ in the combined NO_3^- and NO_2^- pool, suggesting that assimilation and nitrification were co-occurring in surface waters. As stratification progressed, the $\delta^{15}N$ of particulate N below the euphotic depth increased from -5‰ to up to +20‰.

N uptake rates were also influenced by light; based on ^{15}N tracer experiments, assimilation of NO_3^-, NO_2^-, and urea was more rapid in the light (434±24, 94±17, and 1194±48 nmol N L^{-1} day^{-1} respectively) than in the dark (58±14, 29±14, and 476±31 nmol N L^{-1} day^{-1} respectively). Dark NH_4^+ assimilation was 314±31 nmol N L^{-1} day^{-1}, while light NH_4^+ assimilation was much faster, resulting in complete consumption of the ^{15}N spike in less than 7 hour from spike addition. The overall rate of coupled urea mineralization and NH_4^+ oxidation (14.1±7.6 nmol N L^{-1} day^{-1}) was similar to that of NH_4^+ oxidation alone (16.4±8.1 nmol N L^{-1} day^{-1}), suggesting that for labile dissolved organic N compounds like urea, mineralization was not a rate limiting step for nitrification. Our results suggest that assimilation and nitrification compete for NH_4^+ and that N transformation rates throughout the water column are influenced by light over diel and seasonal cycles, allowing phytoplankton and nitrifying microbes to contribute jointly to PNM formation. We identify important factors that influence the N cycle throughout the year, including light intensity, substrate availability, and microbial community structure. These processes could be relevant to other regions worldwide where seasonal variability in mixing depth and stratification influence the contributions of phytoplankton and non-photosynthetic microbes to the N cycle.

1. Introduction

Nitrogen (N) is a limiting nutrient for primary producers in many marine environments, and nitrogen compounds are important energy sources for marine microbes. Nitrogen cycling in the surface ocean involves several key N transformation pathways (**Fig. 1**). The major source of new (external) N is the supply of nitrate (NO_3^-) from deep mixing, advection, or diffusion (Zehr and Ward 2002). N_2 fixation and atmospheric deposition also provide new bioavailable N for phytoplankton growth in some regions (Sañudo-Wilhelmy et al. 2001; Gruber and Sarmiento 1997; Montoya et al. 2004; Duce et al. 2008). Phytoplankton assimilate NH_4^+, NO_3^-, and NO_2^-, collectively referred to as dissolved inorganic N (DIN), into their biomass during autotrophic growth, forming particulate and dissolved organic N (PON and DON) compounds. Organic N is released directly into the environment during cell lysis or excretion, and can be remineralized back to NH_4^+ by microbes during ammonification (Dugdale and Goering 1986; Hollibaugh and Azam 1983; Stepanauskas et al. 1999). To complete the cycle, NH_4^+ is converted first to NO_2^- and then NO_3^- in successive oxidation reactions by different groups of marine nitrifiers during nitrification (Wuchtner et al. 2006; Ward and Carlucci 1985). In turn, NO_3^- can be converted to NO_2^- through incomplete NO_3^- reduction by phytoplankton (Collos 1998), or through photo-reduction (Zafiriou and True 1979). Other N transformation processes like denitrification (Gruber and Sarmiento 1997) and anaerobic NH_4^+ oxidation (Francis et al. 2007) also contribute to N cycling in anoxic marine environments, but generally do not occur in oxygenated waters.

Recent findings have demonstrated that the marine N cycle is more complex than previously understood. For example, certain non-photosynthetic microbes possess genes for NO_3^-, NO_2^-, and NH_4^+ uptake similar to phytoplankton, and are a potentially important "sink" for DIN that is independent of light (Allen et al. 2001; Allen et al. 2005; Cai and Jiao 2008; Starkenburg et al. 2006; Tupas et al, 1994). Likewise, certain phytoplankton utilize DON to satisfy their N demands, similar to heterotrophs (Palenik and Morel 1990; Moore et al. 2002; Zubkov et al. 2003). These findings suggest that more overlap exists in the types of N substrates taken up by phytoplankton and non-photosynthetic microbes than previously believed.

The conditions and setting where the various processes of the N cycle occur has also been expanded. For example, some marine nitrifier populations are inhibited by light, and thus nitrification was thought to be confined to deeper waters (Olsen 1981). However, high nitrification rates within surface waters were observed using ^{15}N tracers (Ward et al. 1989) or calculated using natural abundance ^{15}N and ^{18}O data for NO_3^- (Wankel at al. 2007). Nitrification may therefore occur throughout the water column in some locations.

Despite the complexity of the N cycle, several important characteristics remain apparent. The N cycle comprises numerous N reservoirs (NO_3^-, NO_2^-, DON, etc), and their concentrations and vertical distributions in the water column are affected by physical, chemical and biological factors. Each reservoir may have numerous sources and sinks, some of which have yet to be characterized. Importantly, the dynamic nature of the N cycle, with multiple reactions taking place simultaneously, may result in large fluxes into and out of each reservoir. Yet these fluxes are difficult to quantify by measuring concentration changes alone because the turnover can be very rapid and shuttle N back and forth between reservoirs. Therefore, the standing stock of any N compound in the water column can be constant or very low even though turnover (production and consumption) may be rapid.

Changes in the concentrations of certain N compounds can occur if fluxes into and out of a reservoir become unbalanced. An example of this type of phenomenon is the accumulation of NO_2^- in a stratified water column when NO_2^- production exceeds its consumption, leading to

formation of a primary NO_2^- maximum (PNM, Lomas & Lipschultz 2006). Two mechanisms have been proposed to describe how NO_2^- maxima form. The first entails uncoupled oxidation of NH_4^+ and NO_2^- during nitrification which leads to NO_2^- buildup if the microbial populations responsible for each step are spatially segregated within the water column. This could occur if the populations have different sensitivities to light (Olsen 1981; Guerro and Jones 1996) or different demands for substrate. The second process involves NO_2^- production during incomplete NO_3^- assimilation by phytoplankton, particularly when light stressed (Collos 1998; Lomas and Gilbert 1999; Lomas and Lipshultz 2006). NO_2^- release by phytoplankton could occur if the cell does not receive enough light energy to complete the reduction of NO_2^- into NH_4^+ (Collos 1998), or in response to rapidly changing light conditions, possibly as a photoprotective mechanism (Lomas and Gilbert 2000). Nitrite maxima throughout the world's oceans are generally attributed to one of these two processes (Lipshultz & Lomas 2006 and references therein), although Dore and Karl (1996a,b) showed that vertical separation of reductive and oxidative microbial processes contributes to PNM formation in the Pacific Ocean. Whether these processes co-occur in other locations and, if so, how physical factors influence which process dominates and at what depth in the water column is not clear.

Isotopic analysis of coupled nitrogen ($\delta^{15}N$) and oxygen ($\delta^{18}O$) in NO_3^- can be used for discriminating between biologically mediated N transformation processes, such as those giving rise to the PNM, since each process imparts a unique isotopic signature to both the N and O composition of the sample (Casciotti et al. 2002; Wankel 2006). This is a result of isotope fractionation, which occurs because organisms preferentially take up the light isotopes of O and N, leaving the heavier O and N isotopes in the residual substrate, i.e. NO_3^-. In processes such as assimilation (and denitrification under anaerobic conditions), the $\delta^{18}O_{NO3}$ and $\delta^{15}N_{NO3}$ are viewed to be coupled, as they increase proportionally as NO_3^- is consumed, with an O:N ratio of isotope effects of ~ 1 (Granger et al, 2004 and 2008).

In contrast, nitrification results in the decoupling of $\delta^{18}O$ and $\delta^{15}N$ of nitrate and as a result values will plot along a line with a slope greater than 1. This decoupling is a result of the processes of assimilation and nitrification competing for the NH_4^+ substrate (Wankel 2007). The difference between the isotope effect of nitrification and that of assimilation will determine the isotopic composition of the NO_3^- returned to the N pool. The greater the difference between the isotope effects of the two branching processes, the lower the $\delta^{15}N_{NO3}$ becomes, whereas the oxygen signature is insensitive to the origin of the N in nitrification (Wankel et al. 2007).

The goal of this work is to improve our understanding of the N cycle in the Gulf of Aqaba, Red Sea; a system with nutrient cycles that are similar to many other seasonally stratified subtropical seas (Labiosa et al. 2003). Prior observations in the Gulf have suggested that substrate availability has a strong influence on PNM dynamics, and that nitrification and NO_2^- excretion are dominant in the summer and winter respectively (Meeder et al. in prep). In this study, we seek to improve our understanding of how key physical, chemical and biological processes contribute to this seasonality and identify temporal and spatial trends in N transformation processes and rates. Our approach uses ^{15}N tracer experiments together with natural abundance stable isotope measurements to quantify N transformation rates and determine the extent of N regeneration from organic matter. This combined approach characterizes different pathways in the N cycle over multiple temporal scales under both manipulated (experimental) and *in situ* conditions. Particular attention is given to processes influencing NO_2^- maxima, and formation of the PNM is used as a framework to discuss the different N transformation processes occurring in the Gulf.

2. Materials and Methods

2.1 Field site

The Gulf of Aqaba is a seasonally stratified, subtropical water body extending from the northern Red Sea. During the summer, thermal stratification leads to oligotrophic conditions and picocyanobacteria dominate the phytoplankton community (Lindell and Post 1995; Mackey et al. 2007). During the mixed winter season, mesotrophic conditions prevail, favoring eukaryotic phytoplankton (Lindell and Post 1995). A spring bloom generally occurs in March or April at the onset of stratification, in which eukaryotic phytoplankton typically dominate and are later succeeded by a secondary bloom of *Synechococcus* (Lindell and Post 1995; Mackey et al. 2009). Throughout the year the entire water column is highly oxygenated down to the sea floor.

2.2 In situ sampling

Monthly samples were collected from station A (29°28'N, 34°55'E) in the Northern Gulf of Aqaba as part of a monitoring program (http://www.iui-eilat.ac.il/NMP). Depth profiles were taken using a sampling CTD-Rosette (SeaBird) equipped with 12 L Niskin bottles. Depth profiles were also collected at station A before (March 18) and during (March 24 and 25) the spring bloom in 2008 as the water column transitioned from deep mixing to stratification (we refer to this as "*in situ* bloom monitoring" throughout the text).

2.3 ^{15}N tracer experiments

To quantify N transformation rates, two 1-day ^{15}N tracer experiments were conducted on back-to-back days. Surface water (1 m depth) was collected each day (during the start of the spring bloom) at ~02:00 hr from an offshore station and transported back to IUI within 1 hr. Water was dispensed into acid-washed, sample-rinsed transparent polyethylene bottles (2 L per bottle, 15 bottles per treatment). Isotopically enriched N additions were made from ^{15}N 99 atom % salts (Icon Isotopes) at the following concentrations: 0.1 μmol L^{-1} NO_3^-, 0.1 μmol L^{-1} urea, 0.07 μmol L^{-1} NO_2^-, or 0.005 μmol L^{-1} NH_4^+. NO_3^- and urea were used during the 1st experiment and NO_2^- and NH_4^+ were used in the 2nd experiment. The NO_3^- treatment was repeated on the 2nd day, though only t_0 and t_2 time points were taken (see below for sampling schedule). Control (no addition) bottles were included in both experiments.

For each experiment, ten baseline samples were collected at ~04:00 hr prior to adding the nitrogen spikes. Spikes were administered before dawn at approximately 05:00 hr, and three bottles from each treatment were immediately sampled within 1hr of adding the spike. All remaining bottles (12 per treatment) were incubated in a flow-through tank that maintained ambient surface seawater temperature (~21°C). For each treatment, 6 bottles were incubated in the light under screening material (50% light attenuation), and 6 were incubated in the dark under a black cloth that yielded 100% light attenuation. Three light and three dark bottles were collected for each treatment at two time points. The first time point was at 12:00 hr (7 hours after the tracer was added) and the second time point was at 18:00 hr (13 hours after the tracer was added). Each time point took approximately 1 hr to process. Sub-samples were collected for flow cytometry, total and dissolved nutrients, and particulate and dissolved ^{15}N analyses as described below. Separate dedicated sets of equipment (e.g. funnels, filtration manifolds, forceps, etc) were always used for processing isotopically enriched and control samples. All equipment was acid washed and thoroughly rinsed with seawater prior to use.

Addition of ^{15}N tracer to low nutrient seawater can result in increased uptake rates relative to natural levels following Michaelis-Menten kinetics. We therefore limited our tracer additions to <10% of the ambient concentrations based on measurements of surface water that were taken 1-2 days prior to the experiments. However, measurements of the actual background concentrations for NO_3^- (0.2 μmol L^{-1}), NO_2^- (0.03 μmol L^{-1}), NH_4^+ (0.025 μmol L^{-1}) were lower during the experiment than expected. Our measured rates may therefore overestimate the actual rates by 50%, 230%, and 20% for NO_3, NO_2^-, and NH_4^+, respectively based on Michaelis-Menten kinetics (Dugdale and Goering 1967). Urea concentrations were assumed to be 10% of DON, typical of oligotrophic surface waters (Jackson and Williams 1985; Eppley et al. 1977) and consistent with prior measurements for urea in the Gulf of Aqaba (A. Post, unpublished data). Our measured urea transformation rates could therefore underestimate the actual rates by a maximum of 90% if all DON was urea, however this is highly unlikely.

Despite the potentially large over or under estimates reported above we note that the rates calculated should still be within a typical range of values for the Gulf during this time of year because the ^{15}N additions were based on real concentration levels measured within a few days of the experiment and the phytoplankton composition and abundance did not change significantly over that time (data not shown).

2.4 Particulate nitrogen ^{15}N analysis

Samples for particulate N concentration and isotopic composition were collected for the *in situ* bloom monitoring and for the ^{15}N tracer experiment. Samples were obtained by filtering 1 L aliquots of sample water through pre-combusted (500^oC, 5 hr) 25mm glass fiber filters (GF/F, Whatman). Sample filters were analyzed at the Stable Isotope Facility at University of California, Davis using a PDZ Europa ANCA-GSL elemental analyzer interfaced to a PDZ Europa 20-20 isotope ratio mass spectrometer (IRMS, Sercon Ltd., Cheshire, UK). Sample $\delta^{15}N$ values were calculated by adjusting the measured values using an empirical calibration scale based on laboratory standards. Two laboratory standards (NIST 1547 and acetanilide) were analyzed every 12 samples. Laboratory standards were calibrated against NIST Standard Reference Materials (IAEA-N1, IAEA-N2, IAEA-N3, IAEA-CH7, and NBS-22). The standard deviation of repeated measurements for the method is 0.2‰.

2.5 $\delta^{15}N$ of dissolved inorganic nitrogen

Water samples for dissolved NO_3^- and NO_2^- (N+N) isotopic composition were collected during the *in situ* bloom monitoring and during the ^{15}N tracer experiment. Samples were filtered through pre-combusted (500^oC, 5h) glass fiber filters (GF/F, Whatman) by hand under low pressure using a syringe and Swinnex filter holder. Filtrate was immediately acidified to <pH 3 with trace metal grade hydrochloric acid and stored in the dark at room temperature until analysis. The $\delta^{15}N$ and $\delta^{18}O$ were determined using the method of McIlvin and Altabet (2005). Briefly, the samples were rendered alkaline by addition of excess MgO, and NO_3^- was reduced to NO_2^- by shaking overnight with activated cadmium (Cd). NO_2^- was then reduced to nitrous oxide with sodium azide in an acetic acid buffer for one hour, followed by neutralization with sodium hydroxide and analysis on a continuous flow isotope ratio mass spectrometer (IRMS). Data obtained by this method include contribution from NO_3^- and NO_2^-, which we refer to in the text as N+N for simplicity. The isotopic composition of NO_2^- alone was determined in the ^{15}N tracer experiment samples by omitting the NO_3^- reduction step.

All samples were calibrated and blank corrected using the international isotopic standards USGS 32, USGS 34, and USGS 35 for NO_3^- and three in house standards for NO_2^-. The reference scale for N and O isotopic composition were atmospheric N_2 and SMOW (standard mean ocean water), respectively. Standards were run before, after, and at 12-15 sample intervals during the run. Analytical precision measured from multiple determinations on standards was 0.2‰ for $\delta^{15}N$ and 0.7‰ for $\delta^{18}O$. The detection limit for successful isotopic determination was ~2 nmol N (corresponding to ~130 nmol N L^{-1} based on the volumes of sample we used). For samples falling below this concentration threshold in the ^{15}N tracer experiment, it was possible to increase the N concentration by addition of a known quantity of standard NO_2^- material because introduction of even a small fraction of ^{15}N tracer into the NO_2^- pool would measurably affect the isotopic composition of the mixture. This allowed us to calculate the isotopic composition of the sample from the measured composition of the mixture and the known composition of the standard based on conservation of mass. This process could not be used for natural abundance samples collected during the spring bloom because the isotope signals of the sample and the standards were too similar to determine an accurate value. Therefore, only the isotopic composition of the combined N+N was determined for those samples.

Since NO_2^- was not removed, the Cd reduction method measured the combined isotope composition of NO_3^- and NO_2^- in our samples, and the isotopic values of samples containing a high proportion of NO_2^- will therefore be affected by an analytical artifact. To get a conservative estimate of what the values of $\delta^{15}N_{NO3}$ and $\delta^{18}O_{NO3}$ would be without the NO_2^- signal, two corrections were applied. For O, we assumed that all of the O atoms in NO_2^- exchanged with the seawater for which the abotic equilibrium isotope effect causes the O in NO_2^- to become isotopically enriched by 14‰ relative to the surrounding water (Casciotti 2007). This assumption is valid as samples were acidified immediately after collection and equilibration of oxygen atoms between water and nitrite is rapid at low pH (McIlvin and Casciotti, 2007). This would lead to $\delta^{18}O$ values in NO_2^- of ~15.5-16.5‰ for the Gulf of Aqaba, where the $\delta^{18}O$ of water is 1.5-2.5‰.We then used conservation of mass to determine what the $\delta^{18}O$ would be if no NO_2^- was present by subtracting out its signal using the NO_2^- concentration data. Similarly for N, we calculated what the $\delta^{15}N$ would be if no NO_2^- was present by assuming all of the NO_2^- in the sample was 12.8 ‰ lighter that NO_3^- due to the inverse fractionation effect associated with nitrite oxidation (Casciotti et al. 2010). While nitrification is not necessarily the dominant process throughout the water column, it is likely to be an important process where NO_2^- levels are high, so this assumption provides a conservative yet realistic correction. The $\delta^{15}N$ of the combined

N+N pool may therefore be lighter than expected for NO_3^- alone. The influence of these processes is dependent on the portion NO_2^- in the N+N pool. NO_2^- comprised up to 21% of the N+N in some surface samples from the March 24 and 25 profiles; and the specific implications of this on our data are discussed along with the results. We note that a number of methods are now available to remove NO_2^- from samples prior to analysis (Granger and Sigman 2009) such that the $\delta^{15}N$ of NO_3^- can be measured via the Cd reduction method without this analytical artifact.

2.6 N uptake and transformation rate calculations

N uptake rates were determined from particulate N samples collected at the beginning and end of the ^{15}N tracer experiment. Uptake rates (ρ) were measured for NO_3^-, NO_2^-, NH_4^+ and urea using two equations based on a constant uptake model (Dugdale and Wilkerson 1986):

$$\rho_t = \frac{c_t}{t} \times \frac{{}^{15}N_s - \langle F \rangle}{{}^{15}N_{enr} - \langle F \rangle} \qquad \textbf{(1)}$$

$$\rho_0 = \frac{c_0}{t} \times \frac{{}^{15}N_s - \langle F \rangle}{{}^{15}N_{enr} - {}^{15}N_s} \qquad \textbf{(2)}$$

Where $^{15}N_s$ is the atom% ^{15}N in the sample measured by a mass spectrometer as described above; $^{15}N_{enr}$ is the atom% ^{15}N in the initially labeled pool of NO_3^-, NO_2^-, NH_4^+ or Urea; <F> is the natural abundance of ^{15}N (in atom%); and t is the incubation time. The quantities c_t and c_0 denote the particulate N concentration (μmol L^{-1}) at time t and time zero respectively, and are used to calculate the absolute uptake rate, with units mass per volume per time (nmol N L^{-1} day^{-1}). Equation 1 can underestimate and equation 2 can overestimate the actual uptake rate if there is a significant change in the amount of particulate matter over the course of the experiment (Dugdale and Wilkerson 1986). This effect is small for low uptake rates but can increase as uptake rates increase. We found that values from these equations agreed well for all but our two highest uptake rates. We therefore report an average of ρ_t and ρ_0 as suggested by Dugdale and Wilkerson (1986).

Rates of NH_4^+ oxidation and combined urea mineralization and subsequent oxidation of the NH_4^+ generated were determined from the isotopic composition of NO_2^- measured at the 1 hr time point in the ^{15}N tracer experiment using the following equation:

$$r = \frac{1}{t} \times \frac{{}^{15}N_t c_t - \langle F_{NO2} \rangle c_0}{{}^{15}N_{enr} - \langle F_{NO2} \rangle} \qquad \textbf{(5)}$$

Where r is the net reaction rate, $^{15}N_t$ is the atom% ^{15}N in the sample NO_2^- measured by mass spectrometer as described above for the first time point; $^{15}N_{enr}$ is the atom% ^{15}N in the initially labeled pool of NH_4^+ or Urea; $<F_{NO2}>$ is the natural abundance of ^{15}N of NO_2^- in the baseline sample water (in atom%); and t is the incubation time. The quantities c_t and c_0 denote the NO_2^- concentration (μmol L^{-1}) at time t and time zero (before additions were made), respectively.

Determination of rates based on enrichment experiments is based on the assumption that the labeled fraction represents a constant portion of the total substrate pool throughout the experiment. For example, if $^{15}NO_3^-$ tracer is added as 10% of the background NO_3^- concentration at the start of the experiment, then the atomic percent of $^{15}NO_3^-$ should ideally remain 10% throughout the experiment for accurate measurements to be made. Transformation rates can then

be calculated based on this relationship once the amount of label that gets transformed is measured (e.g. for every one ^{15}N atom taken up, 9 ^{14}N atoms also get taken up). These estimates are subject to error if rapid substrate regeneration occurs (Gilbert et al. 1982; Dugdale and Wilkerson 1986). For example, if NO_3^- is regenerated during an experiment, then the labeled fraction will continually get "diluted" over the course of the experiment. This effect becomes more pronounced in longer experiments. We were unable to quantify dissolved N transformations based on the 7 and 13 hour time points in the ^{15}N tracer experiment because the turnover rates were more rapid than we expected and dilution of the isotope label occurred, thus we use the 1 hour point only.

2.7 Total and Dissolved Nutrients, chl *a* and Irradiance

Total N, NO_3^- and NO_2^- concentrations were collected during all *in situ* monitoring, as well as during the nutrient addition experiment and ^{15}N tracer experiment. Concentrations of NO_3^- and NO_2^- were determined using colorimetric methods described by Hansen and Koroleff (1999) modified for a Flow Injection Autoanalyzer (FIA, Lachat Instruments Model QuickChem 8000) as described previously (Mackey et al. 2007). The precision of the methods was 0.05 μmol L^{-1} for NO_2^- and NO_3^-. The detection limit for these nutrients was 0.02 μmol L^{-1}. Ammonium samples from *in situ* field samples collected during the spring bloom progression were measured using the ortho-phthaldehyde method described by Holmes et al. (1999) with a precision of 0.02 μmol L^{-1} and a detection limit of 0.01 μmol L^{-1}. Total N was determined for March 24 and 25 and for the ^{15}N tracer experiment on whole water samples without filtration. Samples were digested by persulfate oxidation, reduced in a copper-cadmium column, and analyzed colorimatrically following D'Elia et al (1977). The detection limit was 1.4 μmol L^{-1}. Dissolved organic N (DON) was calculated by subtracting the particulate N and total inorganic N (NO_3^- + NO_2^- + NH_4^+) from total N. Photosynthetically available radiation (PAR, 400-700 nm) was measured using a standard high-resolution profiling reflectance radiometer (Biospherical PRR-800, data courtesy D. Iluz). Chl *a* was measured fluorometrically using a Turner Fluorometer (Turner Designs 10-AU-005-CE) following 90% acetone extraction at 0°C for 24 hr as described previously (Mackey et al. 2009).

2.8 Flow cytometry

Flow cytometry was used to determine the abundance of phytoplankton and non-photosynthetic microbes in samples from *in situ* bloom monitoring, the nutrient addition experiment, and the ^{15}N tracer experiment. Samples were preserved with 0.1% glutaraldehyde, flash frozen in liquid nitrogen, and stored at -80°C until analysis. Cell abundances in samples from the *in situ* bloom monitoring and the ^{15}N tracer experiment were measured using a LSRII cell analyzer (Becton Dickinson Immunocytometry Systems, San Jose, CA). Before analysis SYTO 42 blue fluorescent nucleic acid stain (Invitrogen, Molecular Probes) was added at a final concentration of 8 μmol L^{-1} and samples were incubated at room temperature for 5 minutes. The SYTO 42 stain has excitation and emission peaks at 433 nm and 460 nm respectively, and offers strong fluorescence enhancement upon binding nucleic acids such that the fluorescence signal from stained cells is maximized relative to background. Cell populations were identified using 90° light scatter, autofluorescence of photopigments, and SYTO 42 fluorescence. Chlorophyll positive (phytoplankton) cells were identified as *Synechococcus* based on positive phycoerythrin content. *Prochlorococcus*, picoeukaryotes (eukaryotic phytoplankton <2μm in diameter) and nanophytoplankton (phytoplankton >2 μm in diameter) were identified based on their relative

scatter and chlorophyll fluorescence levels. Non-photosynthetic cells were identified based on lack of chlorophyll fluorescence and positive SYTO 42 staining. Cell numbers were determined by spiking each sample with a known concentration of 1μm fluorescent yellow green calibration beads (Polysciences).

3. Results

3.1 *In situ* monthly monitoring

Time series analyses of NO_3^- and NO_2^- depth profiles over representative one-year periods showed a clear relationship with seasonal mixing and stratification (**Fig. 2**). In February 2008 the water column was mixed down to the seafloor before stratification occurred in March (**Fig, 1A**). In the winter (e.g. January-March), NO_3^- and NO_2^- levels were inversely related, with higher NO_2^- levels in the upper mixed layer than at depth. Primary NO_2^- maxima (PNM) began to take shape in March or April, which is the spring season when the water column first begins to stratify. In the summer (e.g. May-September), when the euphotic depth is approximately 100 m, PNM in the stratified water column were evident between 50-200 m. NO_3^- concentrations remained below detection throughout the euphotic zone, and increased gradually with depth below 100 m. This trend is typical of other years, although the actual NO_3^- and NO_2^- concentrations within and below the mixed layer vary with mixing depth. For example in 2003, when the mixing depth was only down to ~400 m, NO_3^- and NO_2^- concentrations differed from those in 2008, but still retained their inverse relationship in the winter and PNM formation the summer (**Fig. 2B**).

Monthly monitoring of chl *a* also showed seasonal changes (**Fig. 2**), with homogenous mixed layer profiles in the winter months and the formation of deep chlorophyll maxima (DCM) between 50-100 m in the stratified summer months. The PNM was located at or below the depth of the DCM in 2008 and 2003.

3.2 *In situ* spring bloom monitoring

To determine how changing physical, chemical, and biological water column characteristics influence N transformation rates, we compared nutrient, chlorophyll *a*, flow cytometry, and isotope data from 3 profiles taken during early stages of stratification in 2008. The first profile was taken when the water column retained many of its characteristics from previous deep mixing. The other profiles were taken on two consecutive days after stratification was established. Prior to the spring bloom in 2008, mixing depths extending to greater than 600 m as judged from nutrient (**Fig. 3A**) and density profiles (not shown).

3.2.1 *Nutrients*

Field sampling conducted on March 18 at the very onset of stratification (**Fig. 3A**) showed nearly homogenous NO_3^- levels (~3 μmol L^{-1}) throughout the water column, with a tendency towards lower concentrations in surface waters (~2 μmol L^{-1}). In surface waters, NO_2^- was higher (0.23 μmol L^{-1-}) than throughout the rest of the euphotic zone (~0.18 μmol L^{-1}), whereas NH_4^+ levels peaked at 100 m (0.42 μmol L^{-1}). Sampling conducted on 24 and 25 March 2008 (**Fig. 3A**) following stratification and during the spring bloom showed continued drawdown of NO_3^- in surface waters, as well as the formation of a PNM peak between 200-250 m (reaching 0.59 μmol L^{-1} at 200 m on 25 March). Maximum NH_4^+ levels occurred above the NO_2^- maxima at depths of 160-200 m, and reached 0.59 μmol L^{-1} at 200 m on 24 March. Particulate N levels increased in surface waters from 0.43 to 2.57 μmol N L^{-1} between March 18-

24, and decreased to 1.08 μmol N L^{-1} by March 25 (**Fig. 3B**). Total N was 12.1 ± 0.7 μmol N L^{-1} (n=21) for all depths in the water column (**Fig. 3C**).

3.2.2 *Phytoplankton growth*

Chl *a* profiles from 18, 24, and 25 March 2008 (**Fig. 3A**) showed the progression of the phytoplankton bloom following stratification. On March 18, the chl *a* profile was homogenous throughout the euphotic zone (~0.2 mg m^{-3}), except in the upper 20 m where it increased to ~0.5 mg m^{-3} **Fig. 3A**). Chl *a* maxima were apparent in both the 24 and 25 March profiles, reaching maximum concentrations of 0.8-0.9 mg m^{-3} between 40-60 m.

Flow cytometry measurements show that by March 24 and 25, phytoplankton populations were most abundant in the upper water column and were dominated by *Synechococcus* and nanophytoplankton (**Fig. 4**). Picoeukaryotes were present in smaller numbers (**Fig. 4**), and no substantial populations of *Prochlorococcus* were identified (data not shown). In the surface, *Synechococcus* reached ~$8.0e^4$ cells mL^{-1} and nanophytoplankton reached ~$2.0e^4$ c mL^{-1}. Both populations increased approximately two-fold between March 24 and 25 between depths of 60-120 m despite being below the 1% light level (60 m). The picoeukaryote population decreased from ~$3e^3$ to ~$0.8e^3$ c mL^{-1} between March 24-25 in surface waters. Non-photosynthetic cells ranged from $5.00e^5$-$2.00e^6$ c mL^{-1} throughout the water column (**Fig. 4**).

3.2.3 *Isotopes of dissolved N+N and particulate N*

Prior to stratification on March 18th the $\delta^{15}N_{N+N}$ and $\delta^{18}O_{N+N}$ were homogenous through the water column, averaging 2.6 ± 0.08 ‰ and 6.7 ± 0.17 ‰, respectively (**Fig. 5A,B**). These values are distinctly different from those expected for average open ocean deep water nitrate $\delta^{15}N$ (5 ‰; Sigman et al. 2000) and $\delta^{18}O$ (2 ‰; Knapp et al. 2008). As stratification progressed and the bloom developed, $\delta^{15}N_{N+N}$ and $\delta^{18}O_{N+N}$ values both increased in surface waters. $\delta^{15}N_{N+N}$ reached peak values of ~10 ‰ at 60 and 20 m on March 24 and 25 respectively (**Fig. 5A**), whereas maximum $\delta^{18}O_{N+N}$ values of 53 and 40 ‰ were seen at the surface (**Fig. 5B**). The $\delta^{15}N$ also showed a subsurface peak of ~11 ‰ at 160 m. These values of $\delta^{15}N_{N+N}$ and $\delta^{18}O_{N+N}$ include an influence from NO_2^-, and may therefore differ from values that would be expected from NO_3^- alone. As outlined above, an isotope mass balance calculation was used to correct for this artifact, the corrected data are plotted in **Fig. 5A and B** along with the actual measured data. The difference between measured and corrected values is greatest for depths in the vicinity of the PNM, and is greater for $\delta^{15}N_{N+N}$ than for $\delta^{18}O_{N+N}$. Despite this limitation, trends in vertical and temporal distributions are larger than can be explained by this artifact alone, hence showing true variability.

The dual isotope plot of $\delta^{18}O_{N+N}$ and $\delta^{15}N_{N+N}$ (**Fig. 6**) shows the tight clustering of values on March 18 as a result of the values being homogenous throughout the water column. If nitrate assimilation was the only process impacting the nitrate pool as stratification progressed, we would expect to see the values sit along a 1:1 line as isotopic fractionation during nitrate assimilation is known to produce a 1:1 increase in the $\delta^{15}N$ and $\delta^{18}O$ of nitrate (Granger et al, 2004). Instead by March 25 the ratios were close to 5:1 (**Fig. 6C**), suggesting a decoupling of the N and O isotopes of nitrate and thus the importance of other processes in addition to nitrate assimilation. We note that the slopes of the $\delta^{18}O_{N+N}$: $\delta^{15}N_{N+N}$ line measured here could be high due to the analytical artifact contributed by NO_2^- in some samples as discussed above. However, although the value of the slopes were not as high overall for any given day in the corrected data set **Fig. 6** (gray circles), the increase in the slopes between days is still apparent.

The $\delta^{15}N$ values of particulate matter on March 18 averaged -4.7 ‰ (**Fig. 5**C). Values increased as stratification was established. Within the upper 100 m, values ranged from 0.8‰ to 6.4‰, and increased with depth, reaching nearly 20 ‰ at 600m.

3.3 ^{15}N tracer experiment

At the start of the ^{15}N tracer experiment the phytoplankton population was dominated by *Synechococcus* ($1.24e^5$ c mL^{-1}), followed by nanophytoplankton ($4.66e^4$ c mL^{-1}) and picoeukaryotes ($4.2e^3$ c mL^{-1}). Non-photosynthetic cells were approximately an order of magnitude more abundant than phytoplankton (~$1.4e^6$ c mL^{-1}). There were no appreciable changes in the community composition of the water used on the 1st and 2nd day of the experiment (not shown).

In order to estimate fluxes of N between different N pools, we used isotope data from the ^{15}N tracer experiment along with nutrient inventory mass balance. We sought to quantify rates for the following N transformations: (1) biological assimilation for NO_3^-, NO_2^-, NH_4^+, and urea; (2) oxidation of NH_4^+ and urea (via NH_4^+ intermediate) to NO_2^- during nitrification; and (3) incomplete NO_3^- reduction to NO_2^- by phytoplankton. The rate of N transfer between two pools can be estimated from tracer experiments if dilution of the ^{15}N label by substrate regeneration is minimal during the experiment, as described above. Dilution of the isotope spike during substrate regeneration generates artificially low rate estimates because the ratio of tracer to unlabeled N becomes smaller than assumed based on initial concentrations of the substrate (i.e., the regenerated substrate "dilutes" the tracer as the experiment progresses). Rates will also be underestimated if the N product formed from the tracer is rapidly consumed by another process. These sources of error can be minimized by selecting appropriate time scales over which to calculate different rates (Gilbert et al. 1982), and these concerns are discussed for each rate estimate below.

3.4 Biological N assimilation

N uptake and assimilation rates were estimated in the ^{15}N tracer experiment based on direct measurements of enrichment in the particulate matter for both light and dark treatments. Error from dilution of the ^{15}N label due to substrate regeneration increases with longer incubation times, as does the likelihood that phytoplankton will excrete and re-assimilate the tracer (Gilbert et al. 1982; Bronk et al. 1994). However, assimilation rates immediately following tracer addition are generally higher than actual *in situ* rates, a problem that can be ameliorated by using a slightly longer incubation time. We used the 1, 7 and 13 hr time points to calculate uptake rates; however, our calculated values could underestimate the actual assimilation rates by a factor of 2 due to dilution of the ^{15}N label from regeneration of substrate (Gilbert et al. 1982), and by 50-74% due to excretion of the ^{15}N label as DON following uptake (Bronk et al. 1994). The background urea concentration during the experiment was 1.0 ± 0.1 μmol L^{-1}. Urea uptake (1194 nmol N L^{-1} day) was approximately three-fold faster than NO_3^- uptake (~434 nmol N L^{-1} day) in the light (**Table 1, Fig. 7A,B**). Both urea and NO_3^- uptake rates were higher in light bottles than in dark bottles (476 nmol N L^{-1} day for urea and 58 nmol N L^{-1} day for NO_3^-, **Table 1, Fig. 7A,B**). For the NH_4^+ treatment, all of the $^{15}NH_4^+$ spike was assimilated prior to the 7 hr sampling in both light and dark bottles, so we only report uptake values based on the 1 hr time point (314 nmol L^{-1} day^{-1}, **Table 1**). For NO_2^-, all of the $^{15}NO_2^-$ was assimilated before the 13 hr sampling; however, based on the 7 hr time point when ^{15}N was still available NO_2^- uptake was three-fold higher in the light (94 nmol N L^{-1} day) than in the dark (29 nmol N L^{-1} day) (**Table 1)**.

N uptake rates at 50% surface PAR were higher for NO_3- (~420 nmol L^{-1} day^{-1}) than for NO_2^- (94 nmol L^{-1} day^{-1}; Table 1). As mentioned above, NO_2^- uptake rates could have been underestimated by 2 fold in the ^{15}N addition experiment; however, even accounting for this potential error, NO_3- uptake still exceeded NO_2^- uptake. We note that the uptake rates could be more similar when NO_2^- concentrations are higher.

3.5 Oxidation of NH_4^+ and urea to NO_2^-

Oxidation rates of NH_4^+ and urea (following mineralization to NH_4^+) were determined based on measurements of NO_2^- isotopic composition after ^{15}N enriched spikes of NH_4^+ or urea were added in the ^{15}N tracer experiment. We calculated rates for the 1hr time point, but were unable to quantify rates from the 7 and 13 hr time points because the ^{15}N enrichments were too small or the turnover of the N pools was too rapid for accurate estimates to be made over these longer time scale (substrate regeneration affected the results). Oxidation of NH_4^+ to NO_2^- occurred at a rate of 16.4±8.1 nmol N L^{-1} d^{-1} (or 0.68±0.34 nmol N L^{-1} hr^{-1}). Mineralization of urea to NH_4^+ with subsequent oxidation to NO_2^- occurred at a rate of 14.1±7.6 nmol N L^{-1} d^{-1} (0.59±0.32 nmol N L^{-1} hr^{-1}; **Table 1**).

3.6 Reduction of NO_3^- to NO_2^-

We were unable to measure reduction of NO_3^- to NO_2^- based on data from the ^{15}N tracer experiment. For the 7 and 13 hr time points, substrate regeneration caused dilution of the ^{15}N label during the experiment and precluded accurate calculations from being made. In addition, since reduction of NO_3^- to NO_2^- is driven by light, we were unable to measure this process in samples from the 1 hr time point, because the samples were collected before dawn and received no light to initiate this process. Therefore, the rate of NO_3^- reduction based on the 1 hr time point in the ^{15}N tracer experiment was negligible, as expected.

However, incomplete reduction of NO_3^- and release of NO_2^- by light limited phytoplankton is a well documented phenomenon in both field and culture studies (Collos 1998; Lomas and Lipschultz 2006 and references therein). The rate of NO_3^- reduction to NO_2^- by phytoplankton is dependent on light and on phytoplankton abundance. Therefore, if phytoplankton were a significant source of NO_2^- in a certain portion of the water column following stratification, then we would expect the change in NO_2^- concentration to be correlated with both light and chlorophyll abundance over those depths. We therefore calculated a range of net NO_2^- formation rates based on changes in the *in situ* NO_2^- concentrations measured during the spring bloom between March 18-24, and tested if they were correlated with irradiance or chl *a* concentrations. These NO_2^- formation rates are "net accumulation" rates, and represent the combined input from all NO_2^- sources (e.g. phytoplankton or NH_4^+ oxidation) as well as all NO_2^- sinks (e.g. assimilation or NO_2^- oxidation). While all of these processes can potentially influence the calculated rate at each depth, light and chlorophyll abundance will correlate most strongly with NO_2^- formation over depths where incomplete reduction of NO_3^- and expulsion of NO_2^- by light limited phytoplankton is the dominant process.

We found that net NO_2^- formation was strongly correlated with light between 60-200 m (R^2=0.99, **Fig. 8B, Table 2**) and ranged from 2.2-58 nmol L^{-1} day^{-1} (0.092-2.4 nmol L^{-1} hr^{-1}). Chl *a* concentration was also correlated with NO_2^- formation rates; however, this relationship was primarily because chl *a* abundance is also controlled by light (**Fig. 8C**). To parse the independent effect of chl *a* concentration on NO_2^- formation rate, we compared the residual chl *a* and NO_2^- formation rate data after subtracting out the influence of light on each parameter according to the

following procedure.

The influence of light on each parameter (chl *a* concentration or NO_2^- formation rate) was calculated based on the equations best fit as shown in **Fig. 8B** and **C**. The calculated value was subtracted from the actual measured value to obtain the residual value. The residual values are the portions of the actual chl *a* and net NO_2^- formation rate measurements that are not accounted for by light. The residual values of chl *a* and net NO_2^- formation rate were then plotted (**Fig. 8D**) to determine the relationship between chl *a* and net NO_2^- formation rate. With the exception of one outlier point (showing a lower NO_2^- formation rate than expected), a strong linear relationship existed between residual chl *a* levels and residual NO_2^- formation rates (**Fig. 8D**). Interestingly, the outlier point coincided with an NH_4^+ peak at 120 m that got consumed between March 18 and 24 (**Fig. 3A**). The NO_2^- formation rate at this depth did not correspond to chl *a* because a larger portion of the NO_2^- at that depth was likely formed by NH_4^+ oxidation. If all of the NH_4^+ drawn down at this depth between March 18-24 was oxidized to NO_2^- it would have contributed ~115 nmol NO_2^- L^{-1}, or approximately 80% of the NO_2^- inventory at that depth, enough that the NO_2^- formation rate would no longer be correlated with chl *a* (e.g. because it is generated by non-photosynthetic microbes instead of phytoplankton). While the net NO_2^- formation rate we calculated for 120 m contains some non- quantified input from NH_4^+ oxidation, the robust correlations between NO_2^- formation and light and chl *a* at the other depths between 60-200m strongly suggest that NO_3^- reduction was the dominant NO_2^- forming process at these depths. However, the net NO_2^- formation rates we report are not necessarily equivalent to NO_3^- reduction rates by phytoplankton; they likely underestimate real NO_3^- reduction rates because they do not account for processes that remove NO_2^-, such as NO_2^- oxidation during nitrification.

4. Discussion

The Gulf of Aqaba has predictable seasonal patterns of NO_2^- distribution, and the spring bloom is a period in which water column N dynamics transition between two different steady states. The changing physical, chemical, and biological characteristics of the water column during the onset of stratification in 2008 gave rise to substantial changes in the N cycle such that new steady state nutrient inventories were established. As the water chemistry shifted toward this new steady state different processes became dominant, giving rise to a PNM over a period of several days. Below we discuss these changes in the N cycle and how they lead to formation of the PNM which is maintained throughout the summer stratified period.

4.1 NO_2^- dynamics during the transition from mixing to stratification

The persistence of NO_2^- in the ocean results from an imbalance in the processes that produce and consume NO_2^- (**Fig.1**). In the aerobic water column, NO_2^- is produced by NH_4^+ oxidizing organisms during the first step of nitrification, and by phytoplankton during incomplete NO_3^- assimilation. It is consumed by NO_2^- oxidizers during the second step of nitrification, and by phytoplankton during assimilation. Nitrite accumulates when production exceeds consumption as long as dispersion rates are sufficiently low. In the Gulf of Aqaba in winter, NO_2^- is present at measurable concentrations throughout the mixed layer, whereas in the summer NO_2^- accumulates below the euphotic zone, forming a PNM (**Fig. 2;** Al-Qutob et al. 2002; Meeder et al. submitted).

To determine the role of phytoplankton in NO_2^- formation, we considered the following three observations. First, *in winter* NO_2^- *was observed throughout the mixed layer, which is the*

*depth of the water column occupied by phytoplankton, regardless of the exact mixing depth (**Fig 1**). NO_2^- did not accumulate below the mixing depth where phytoplankton do not survive.* The mixed layer is the portion of the water column homogenized by turbulent mixing; for example, the mixed layer extended to the sea floor (~700m) in February 2008 (**Fig. 2A**), and to ~250 m in February 2003 (**Fig. 2B**). Phytoplankton can inhabit the whole mixed layer because water periodically gets mixed to the sunlit surface waters and allows for photosynthesis to occur (Smayda and Mitchell-Innes 1974); they cannot grow in the permanent darkness of the deep water below the mixing depth. NH_4^+ oxidizers, on the other hand, can occupy and grow throughout the entire water column including deep waters below the mixing depth because they do not require sunlight to survive. Therefore, if the major source of the NO_2^- in winter were NH_4^+ oxidizers, then the accumulation of NO_2^- would not be confined exclusively to the mixed layer, as we observe (**Fig. 2**). Second, *the inverse relationship between NO_3^- and NO_2^- in winter profiles is maintained regardless of shoaling or deepening of the mixed layer during winter (**Fig. 2**).* This correlation suggests that NO_3^- is the source of NO_2^- generated within the mixed layer because as NO_3^- is consumed NO_2^- is produced. Third, *the NO_2^- and NO_3^- inventories in the winter mixed layer agree well with the ratios of NO_2^- to NO_3^- observed during excretion by light limited phytoplankton following NO_3^- uptake*. Specifically, the fraction of NO_2^- generated relative to NO_3^- consumed in the mixed layer ranged from ~10% in 2003 (where ~0.4 μmol NO_2^- L^{-1} was generated and 4-6 μmol NO_3^- L^{-1} was consumed; **Fig 2A**) to ~15% in 2008 (where ~0.3 μmol NO_2^- L^{-1} was generated and 2 μmol NO_3^- L^{-1} was consumed; **Fig. 3A**). These ratios are consistent with the range of ratios measured in cultures of light limited phytoplankton that expel a portion of the NO_3^- they take up as NO_2^- (Collos 1998 and references therein). The non-nutritional uptake of NO_3^- and release of NO_2^- may be a mechanism by which certain phytoplankton regulate photosynthetic electron flow during periods when irradiance fluctuates (Lomas and Gilbert 1999, 2000), e.g. during deep mixing. Based on the above observations, phytoplankton appear to be the major source of NO_2^- during convective winter mixing. These findings agree with an incubation study by Al-Qutob and co-workers (2002), in which NO_2^- was produced by phytoplankton following N additions, and with monitoring studies conducted in this region (Meeder et al. in press).

In a mixed water column, biological N transformation rates reflect the "average" light conditions because their products get distributed over the entire mixed layer. During winter in the Gulf of Aqaba, the mixing time (e.g. the time required for a parcel of water to complete one cycle of mixing from surface to the mixing depth and back to surface) is approximately 14 hr, 22 hr, and 29 hr for mixing depths of 200 m, 400 m, and 600 m respectively based on typical heat flux and wind stress values for the region (S. Monismith, personal communication). The homogeneity of NO_2^- in the mixed layer suggests that the mixing time is fast relative to the rates of NO_2^- production and consumption such that no localized accumulation or drawdown of NO_2^- is observed in the mixed layer.

In contrast, in a stratified water column organisms at any given depth are subject to relatively predictable light regimes. This allows different groups of organisms to populate depths they are best adapted to occupy. The PNM forms when stratification imposes a range of physical and chemical gradients on organisms, allowing different steady states to be reached between NO_2^- production and consumption at different depths in the water column. This is evident from summer profiles of NO_2^- from 2003 and 2008, where NO_2^- accumulates at ~100 m, but not in surface or deep waters. These monthly "snapshots" provide information on steady state nutrient levels; they integrate and reflect the net result of all processes that produce and consume NO_2^- at

a given depth.

The individual contributions of specific N transformation processes on PNM formation can be discerned from the higher frequency monitoring data collected during the spring bloom. To focus our discussion, we define four principal regions of the water column based on light attenuation and major features of the PNM (**Fig. 9**). The "euphotic zone" (0-60 m during our study), extends from the surface to the compensation depth (i.e., the depth at which light is attenuated to 1% of surface irradiance). The "sub-euphotic zone" (60-160 m during our study), extends to the top of the PNM. The "upper PNM" (180-225 m during our study), encompasses depths with substantial accumulation of NO_2^-. The "disphotic zone" extends from the depth where the NO_2^- concentrations of the PNM starts decreasing down to the sea floor (below 225 m during our study). We note that the absolute depths given above for our study are not universal for all summers in the Gulf of Aqaba or for all water columns because they would change depending on the depth of the mixed layer prior to stratification, latitude, amount of chl *a* present, and other factors influencing light penetration. Below we describe how N cycling processes that produce and consume NO_2^- generate conditions that give rise to the PNM.

4.1.1 Euphotic zone.

The euphotic zone is the layer in which sufficient light is available for photosynthesis to exceed respiration, and where the majority of photosynthetic biomass is generated. Uptake of NO_3^- and NH_4^+ is at times light dependent in natural phytoplankton populations, with the highest rates generally occurring in the surface ocean and decreasing with depth as light becomes attenuated (MacIsaac and Dugdale 1972). This trend was observed in the euphotic zone of the Gulf as stratification became established. DIN uptake by phytoplankton was highest in surface waters and lower at the base of the euphotic zone (**Fig. 3A**).

Most of the available NO_3^- and NO_2^- in the euphotic zone of the Gulf of Aqaba was assimilated and converted into biomass (e.g. photosynthetic uptake) (**Fig. 3)** between March 18 and 25. However, results suggest that mineralization and subsequent nitrification of organic N played an important role in the euphotic zone, where DIN concentrations were low due to efficient phytoplankton uptake. Between March 18 and March 25 $\delta^{15}N_{N+N}$ increased by 8 ‰ in comparison to 45 ‰ for $\delta^{18}O_{N+N}$ (most enriched values seen on March 24) in surface samples (e.g., upper 20m), causing high $\delta^{18}O_{N+N}$: $\delta^{15}N_{N+N}$ ratios relative to the rest of the water column on March 24 and 25. The increasing slope of $\delta^{18}O_{N+N}$: $\delta^{15}N_{N+N}$ (up to 5) indicates decoupling of the N and O isotopes of nitrate, which suggests an important role for assimilation and recycling, e.g. nitrification, in the euphotic zone. The decoupling is a result of the branching during NH_4^+ consumption in which NH_4^+ serves as a substrate for regenerated production and for nitrification. The difference between the isotope effects of these two processes controls the $\delta^{15}N$ of the NO_3^- returned to the N pool, whereas the O is insensitive to the origin of the N (Wankel et al, 2007). This greater enrichment of O relative to N due to co-occurring assimilation and nitrification has also been observed in surface waters in Monterey Bay (Wankel et al. 2007), where regenerated N supports 15-27% of NO_3^- based production.

$\delta^{15}N_{N+N}$ and $\delta^{18}O_{N+N}$ can be affected by factors other than assimilation and nitrification, such as those that contribute NO_3^- with different isotopic compositions than deep water N+N. For example, atmospheric dry deposition has been shown to be a substantial contributor of relatively light N and heavy O to the Gulf of Aqaba (summer average $\delta^{15}N$ -1.7 ‰ and $\delta^{18}O$ 77.3‰; Wankel et al. 2009). Another potential source of light N in surface water (**Fig. 5A**) is biological N_2 fixation, which reflects the $\delta^{15}N$ of atmospheric N_2 gas that is by definition zero.

Measurements of N_2 fixation rates in the Gulf have ranged from below detection (Hadas and Erez 2004) to low but measurable rates of 1-2 nmol L^{-1} day^{-1} (Foster et al. 2009). These rates are small compared to other N transformation rates measured for the Gulf (**Table 1**). However, we did not measure N_2 fixation or atmospheric deposition directly in this study, so a contribution from either cannot be confirmed or ruled out. Preferential export of ^{15}N in particulate matter out of the euphotic zone (Altabet 1988) can skew the $\delta^{18}O_{N+N}$: $\delta^{15}N_{N+N}$ relationship in surface waters, and is apparent from the increased $\delta^{15}N$ of particulate N with depth as the bloom progressed (**Fig. 5C**), although fractionation during mineralization could also contribute to this signal.

4.1.2 Sub-euphotic zone.

In this zone light is attenuated below the compensation threshold, and respiration by the entire microbial community is likely to exceed photosynthesis by phytoplankton. Regression analysis for depths in the sub-euphotic zone and down to 200 m showed that net NO_2^- production rates correlated very strongly with decreasing irradiance (**Fig. 8B**). However, regression analysis of residual chl *a* and residual NO_2^- production data (i.e. with the influence of irradiance removed) also showed a remarkably strong correlation (**Fig. 8D**), and suggested that NO_3^- uptake and released as NO_2^- by light limited phytoplankton was the dominant N transformation process in the sub-euphotic zone during the beginning of the bloom (March 18-24). These results agree with the findings of Dore & Karl (1996a) in the Pacific Ocean, where they suggest that the upper portion of the PNM is generated by phytoplankton NO_2^- release and closely tracks the nitricline.

An exception occurred at 120 m, where a large portion of NO_2^- was generated from NH_4^+ oxidation rather than NO_3^- reduction based on regression statistics (**Fig. 3A; Fig. 8D**). The contribution of NH_4^+ oxidation to the NO_2^- formation over this range of depths suggests that substrate limitation of NH_4^+ oxidation rates may be impacting NO_2^- distribution in the water column (Ward 1985). Our data shows that NO_2^- formation from NH_4^+ oxidation can match or exceed NO_3^- reduction where ample NH_4^+ is available. Indeed, the increasing slope of the best fit line for $\delta^{18}O_{N+N}$: $\delta^{15}N_{N+N}$ over this range of depths (Fig. 6, orange circles) indicates that nitrification was occurring within the sub-euphotic zone.

While the sub-euphotic zone is below the compensation depth, it is important to note that phytoplankton continue to take up nutrients and perform photosynthesis in this dim layer (these rates are simply exceeded by respiration rates). The $\delta^{15}N_{N+N}$ was elevated in the sub-euphotic zone with respect to deeper water as the bloom progressed (**Fig. 5A**), indicating that assimilation of N+N by phytoplankton or other microbes takes place. While seemingly counterintuitive that phytoplankton could be both a source and a sink for NO_2^- in the sub-euphotic zone over the course of a bloom, several processes could lead to this outcome. First, intermittent changes in light intensity due to internal waves could lead phytoplankton at the base of the sub-euphotic zone to toggle between NO_3^- assimilation and NO_2^- excretion depending on their light requirements. Another factor is that the phytoplankton community is a diverse assemblage of different sub-populations, each with its own light requirements and N assimilation strategies. During the bloom succession occurs within the phytoplankton community, and different sub-populations coexist, compete, and eventually either survive or get out-competed. Therefore, while one sub-population may take up NO_3^- and release NO_2^- due to light limitation, another may be able to complete the assimilation of NO_3^- into biomass. Between March 24-25 nanophytoplankton abundance increased in the sub-euphotic zone (**Fig. 4**). Nanophytoplankton include phytoplankton taxa such as diatoms, and monitoring conducted after our sampling period showed that the spring bloom became dominated by diatoms by the beginning of April (Iluz et

al. 2009). Non-nutritional uptake of NO_3^- has been observed in some marine diatoms (Lomas and Gilbert 1999), and uptake (though not necessarily assimilation) by these comparatively large cells may have played a role in the drawdown of NO_3^- and NO_2^- in the sub-euphotic zone. Light-independent assimilation of NO_3^- and NO_2^- by non-photosynthetic microbes, which were abundant throughout the water column, could also have caused the high $\delta^{15}N_{N+N}$ values at these dim depths (Tupas et al. 1994).

4.1.3 The upper PNM.

The upper PNM (180-225 m) is a dynamic region where NO_2^- accumulates. Within this layer light is attenuated to levels too low for photosynthesis (**Fig. 8A**). During the first part of the bloom NO_2^- dynamics in the upper PNM were similar to the sub-euphotic zone in that NO_2^- production was strongly correlated with chl *a* levels, implicating phytoplankton as the main source of NO_2^- (**Fig. 8**). However, over the next day, net NO_2^- production continued within the upper region of the PNM and was no longer correlated to chl *a* (data not shown). The NO_2^- produced by phytoplankton during the first part of the bloom was derived from NO_3^- taken up during the mixed period (e.g. March 18) when, due to mixing, light was episodically high enough to support NO_3^- uptake. Following stratification phytoplankton trapped below the euphotic depth would have expelled that N as NO_2^- due to a lack of light energy needed to complete the assimilation process. However, by March 24 phytoplankton trapped within the upper PNM would have been without sufficient light for approximately one week. It is unlikely that these cells could initiate de novo uptake of fresh NO_3^- and be the source of NO_2^- generated at this depth between March 24 and 25. NH_4^+ oxidizers, on the other hand, would have access to an increasingly large pool of DON from which to access their NH_4^+ substrate following ammonification.

NO_2^- can only accumulate if production exceeds consumption and dispersion is sufficiently low. The NO_2^- accumulation in the upper PNM (180-225 m) during the second part of the bloom indicates that NO_2^- production and consumption were decoupled, with production exceeding consumption. Nitrification was the major source of NO_2^- in the upper PNM once phytoplankton NO_2^- excretion had declined following the initial stages of stratification. The main NO_2^- consuming process at these depths was NO_2^- oxidation because photosynthetic NO_2^- assimilation is light limited at these dark depths. The steep slope of $\delta^{18}O_{N+N}$: $\delta^{15}N_{N+N}$ values for N+N shows that nitrification was occurring over this range of depths by March 25 when stratification was firmly established (Fig. 6, green circles). Olsen (1981) postulated that the greater sensitivity of NO_2^- oxidizers than NH_4^+ oxidizers to light could be a mechanism by which PNM form. Guerrero and Jones (1996) added to this model, noting that NH_4^+ oxidizers recover more rapidly from photoinhibition than do NO_2^- oxidizers. Based on these observations, NH_4^+ oxidizers are postulated to be more active in shallower regions of the water column than NO_2^- oxidizers, and this spatial segregation of the populations leads to accumulation of NO_2^-.

The pattern of PNM formation in the Gulf of Aqaba is consistent with these hypotheses of differential photoinhibition and recovery based on the concentrations of NH_4^+, NO_2^-, and NO_3^- throughout the water column. The NO_3^- concentration data suggests that NO_2^- oxidation was closely coupled to NH_4^+ oxidation *only* at depths below ~225 m, where production of NO_3^- was observed concurrently with NH_4^+ and NO_2^- consumption (**Fig. 3A**). At these dark depths no NO_2^- accumulated, consistent with a lack of photoinhibition of either NH_4^+ or NO_2^- oxidizers. In contrast, above the upper PNM (140-180 m) NH_4^+ accumulated and resulted in an NH_4^+ peak by March 25. The light levels at these depths may have been sufficiently high to inhibit NH_4^+

oxidation rates in keeping with the hypotheses discussed above, thereby allowing NH_4^+ to accumulate. However, within the upper PNM depths of 180-225m, NO_3^- and NO_2^- accumulated concurrently, suggesting that NH_4^+ oxidation was continuing while NO_2^- oxidation was slowing, an observation that could be explained by differential photosensitivity of the two nitrifier populations. However, recovery from photoinhibition must have been reversible over the diel cycle, as the isotope data strongly indicate a complete nitrification cycle within the euphotic zone and upper PNM in the Gulf of Aqaba.

4.1.4 The Disphotic Zone.

The disphotic zone contains the lower portion of the PNM (225-300 m; **Fig. 3A**) as well as deep water. Within the disphotic zone, sunlight is attenuated to less than 0.001% of surface irradiance and phytoplankton are unable to perform photosynthesis. Therefore, non-photosynthetic microbial processes dominate the N cycle at these depths, and indeed, several observations are indicative of a nitrification-dominated system. As noted above, NH_4^+ and NO_2^- were consumed while net NO_3^- production occurred below 225 m, consistent with microbially mediated oxidation of NH_4^+ and NO_2^- into NO_3^-. Microbial nitrification in the disphotic zone also refined the shape of the lower PNM during the onset of stratification by consuming a portion of the broad band of NO_2^- that was generated during the beginning of stratification, and helped maintain the characteristic shape of the PNM throughout the summer. This can be seen on March 25, where the falling limb of the PNM took on a steeper slope than on March 24 (**Fig. 3A**) and was more similar to summer profiles from other years (**Fig. 2**).

The elevated $\delta^{15}N$ of particulate N that was spread throughout the water column by March 25 (**Fig. 5C**) also suggests that a link exists between phytoplankton growth in the surface and mineralization/nitrification at depth. Active processes, such as selective zooplankton grazing and excretion, play an important role in packaging smaller suspended particles, such as phytoplankton cells, within the euphotic zone for export as sinking particles. As a result, sinking particles are generally higher in $\delta^{15}N$ than suspended particles within the euphotic zone (Altabet 1988). The transport of sinking particles occurred quickly, as the elevated $\delta^{15}N_{part}$ was already spread throughout the water column within days of the bloom initiating (**Fig. 5C**). The sinking of particulate matter from the surface to deep water is likely to be an important source of N that fuels nitrification in the disphotic zone throughout the stratified period, and recharges the NO_3^- reservoir at depth.

Values for $\delta^{15}N_{N+N}$ and $\delta^{18}O_{N+N}$ in the disphotic zone varied little over the time period studied ($\delta^{15}N_{N+N}$ was ~2.5 and $\delta^{18}O_{N+N}$ was ~6.5), but were distinct from those observed for open ocean deep water nitrate; ($\delta^{15}N$ 5 ‰ (Sigman et al. 2000) and $\delta^{18}O$ 2 ‰ (Knapp et al. 2008). Low $\delta^{15}N$ with respect to deep water NO_3^- has also been observed in the Mediterranean Sea (Pantojo et al, 2002). Potential causes include ^{15}N depleted sources such as N_2 fixation and atmospheric deposition along with the lack of water column denitrification and its associated large isotope effect (~25 ‰, Cline and Kaplan, 1975) and the restricted exchange of these systems with the open ocean. The higher $\delta^{18}O_{N+N}$ values may be partially due to the higher $\delta^{18}O$ of water in the Gulf of Aqaba corresponding to its elevated salinity, and on a regional scale the higher $\delta^{18}O$ signal in water would be transferred to NO_3^- via nitrification (Casciotti et al, 2010). Atmospheric deposition in this region is another source of NO3- with higher $\delta^{18}O_{N+N}$ (Wankel et al. 2009).

4.2 N uptake and regeneration in the Gulf of Aqaba

Our measurements for uptake of NO_3^- (26-434 nmol N L^{-1} day^{-1}) and NH_4^+ (314 nmol N L^{-1} day^{-1}) are in good agreement with uptake estimates from other studies for NO_3^- (ranging from 48-526 nmol N L^{-1} day^{-1}) and NH_4^+ (40-1536 nmol N L^{-1} day^{-1}) in a range of environments and for different light intensities (Bronk et al. 1994; Wheeler and Kirchman 1986; Probyn and Painting 1985; McCarthy 1972). Fewer measurements of NO_2^- uptake are available; however, an approximation can be made based on the cell specific NO_2^- uptake rate determined for Synechococcus 7803 (0.02 fmol $cell^{-1}$ hr^{-1}; Lindell et al. 1998). This would correspond to a NO_2^- uptake rate of ~80 nmol N L^{-1} day^{-1} based on the phytoplankton cell abundances measured during our study (~1.70e^5 c mL^{-1}), and is consistent with the range of uptake rates we measured in our ^{15}N tracer experiment (29-94 nmol N L^{-1} day^{-1}). Urea uptake rates encompass a much broader set of values in the environment, ranging from <2.4 to 86,400 nmol N L^{-1} hr^{-1} (Kristiansen 1983, Berg et al. 1997, Lomas et al. 2002, Berman & Bronk 2003), and our measured rates of 296-1285 nmol N L^{-1} hr^{-1} fall within that range. We note that spontaneous decomposition of urea into NH_4^+ can occur in the light and were determined to be ~240 nmol L^{-1} day^{-1} in the Gulf of Aqaba (Kamennaya et al. 2008). However, this rate was measured following a relatively concentrated urea spike of 20 μmol N L^{-1}, compared to our dilute spike of 0.2 μmol N L^{-1}. If degradation kinetics are similar over this range of urea concentrations, then spontaneous degradation of urea to NH_4^+ could have caused an overestimation of ~20% for our urea uptake rates in the light.

The N cycle in the Gulf of Aqaba provides an example of a system with closely coupled N assimilation and regeneration during the stratified period. The increasing slope of the best fit line for $\delta^{18}O_{N+N}$: $\delta^{15}N_{N+N}$ (from 2:1-5:1; **Fig. 6**) indicates that regenerated organic matter is a major source of N for primary producers in the Gulf of Aqaba, because it shows a strong signature of uncoupled fractionation of N and O that is imparted during nitrification. This observation is consistent with other studies that have found high rates of primary productivity despite relatively low standing stocks of phytoplankton in the Gulf (Hase et al. 2006). Together these findings suggest that assimilation and nitrification compete for NH_4^+, and that primary productivity is tightly coupled to grazing food webs and microbial remineralization processes, which are a source of NH_4^+. Productivity is therefore partially supported by efficient sequestration of NH_4^+ within cells as soon as it becomes available, in addition to using NO_3^- produced during nitrification.

During our monitoring of the spring bloom the concentration of DON increased by 1.1 μmol N L^{-1} as DIN decreased by this amount (**Fig. 3B**). Labile DON could play an important role in the Gulf's biogeochemical cycling of N and serve as an important nutrient resource for non-photosynthetic microbes and marine phytoplankton, similar to other areas of the ocean (Solomon et al. 2010; Palenik and Morel 1990; Moore et al. 2002; Zubkov et al. 2003. The role of labile DON could be particularly important in ultra-oligotrophic marine environments where DIN concentrations are very low and the reservoir of DON can be over an order of magnitude larger than DIN, as was the case in the Gulf of Aqaba where DON reached ~10 μmol N L^{-1} and the NO_3^- concentration was 0.1-0.2 μmol L^{-1} (March 25). Moreover, in some marine diatoms NH_4^+ and DON uptake rates increase with temperature while NO_3^- uptake rates decrease (Lomas and Gilbert 1999), suggesting that DON could be the preferred source of N for phytoplankton that bloom in warming surface waters as stratification becomes established.

In the Gulf of Aqaba where ammonification and nitrification are closely coupled, NH_4^+ generated during mineralization of DON should be considered when making measurements of NH_4^+ oxidation. Calculations based on ^{15}N labeling data are complicated by rapid and closely

coupled NH_4^+ production and consumption, and can result in rate underestimation. In this study the rate of coupled mineralization and NH_4^+ oxidation were measured in the ^{15}N tracer experiment for urea, a labile form of DON. The overall rate of coupled urea mineralization and NH_4^+ oxidation (14.1 nmol N L^{-1} day^{-1}) was remarkably similar to that of NH_4^+ oxidation alone based on our study (16.4 nmol N L^{-1} day^{-1}) and other studies (~18-40 nmol N L^{-1} day^{-1}; Ward 2005; Ward et al. 1982), suggesting that mineralization is not a rate limiting step for nitrification, at least when the DON pool is relatively large and labile. The composition and lability of DON changes based on community composition, grazing rates, mixing, and numerous other factors, although estimates suggest that complete DON turnover occurs on the order of 10 days in oligotrophic waters (Bronk et al. 1994). Rates measured for labile DON compounds, such as urea in this study, provide maximum potential rates for DON mineralization and nitrification. Actual rates will be lower, and mineralization may limit nitrification rates for NH_4^+ derived from more refractory forms of DON. More work is needed to characterize the DON pools in different waters and determine their influence on marine nitrification rates.

5. Conclusion

This study used isotope data from natural abundance samples in the Gulf of Aqaba together with tracer experiments to identify important processes in the N cycle and quantify their rates. The approach has highlighted the importance of regenerated N for supporting productivity in the Gulf of Aqaba, where efficient photosynthetic sequestration of N in surface waters is coupled to mineralization and nitrification of PON and DON throughout the water column. Export and regeneration (mineralization and nitrification) of particulate N to DIN at depth serves to recharge the NO_3^- reservoir in deep water.

Several major light-sensitive processes contribute to the formation of PNM in the Gulf of Aqaba during the transition from mixing to stratification. Within the euphotic zone, phytoplankton assimilate N during growth by drawing down DIN levels sharply in the well-lit surface waters. Below the euphotic depth during the initial stages of stratification, a large inventory of NO_2^- is generated from incomplete NO_3^- reduction by trapped, light limited phytoplankton. NO_2^- from this process is distributed over a range of depths, creating a broad band of NO_2^- with a subsurface peak. Later, once stratification is firmly established, net NO_2^- is generated by NH_4^+ oxidizers over a narrower range of depths coinciding with the upper part of the PNM, and is consistent with differential light inhibition of NH_4^+ and NO_2^- oxidizing communities. Deeper in the water column where light is negligible, NO_2^- oxidation rates match NH_4^+ oxidation, and NO_2^- gets drawn down, defining the lower portion of the PNM.

Mineralization and subsequent nitrification of organic material is an important source of N for primary producers in the Gulf of Aqaba, where NO_3^- formed from nitrification of NH_4^+ and urea (following ammonification) at rates of similar magnitude. The similar magnitudes of assimilation rates for urea and NO_3^- suggest that labile organic N is an important source of N for primary producers in this oligotrophic region during the stratified season. The rate and type of N transformation processes operating throughout the water column are strongly influenced by light, which determines the maximum depths for net photosynthesis and may contribute to inhibition of nitrifying communities.

Table 1: N transformation rates determined in the ^{15}N tracer experiment. N assimilation rates into particulate biomass for NO_3^-, NO_2^-, urea, and NH_4^+, as well as NO_2^- formation rates from NH_4^+ and urea are shown. "N addition" indicates the form of ^{15}N enriched spike added. "Light" uptake rates indicate bottles incubated at 50% surface sunlight irradiance, and "dark" uptake rates indicate bottles incubated in full darkness.

N addition	Process	Experiment number	Time (hr)	Light rate (nmol N L^{-1} day^{-1})*	Dark rate (nmol N L^{-1} day^{-1})*
NO_3	assimilation	1	1	ND	26±0.00
NO_3^-	assimilation	1	7	434±24	58±14
NO_3^-	assimilation	1	13	415±103	65±19
NO_3^-	assimilation	2	1	ND	41±2.4
NO_3^-	assimilation	2	13	420±82	137±79
NO_2^-	assimilation	2	1	ND	29±12
NO_2^-	assimilation	2	7	94±17	29±14
NO_2^-	assimilation	2	13	ND	ND
Urea	assimilation	1	1	ND	296±40
Urea	assimilation	1	7	1194±48	476±31
Urea	assimilation	1	13	1285±32	308±10
Urea	remineralization and oxidation to NO_2^-	1	1	ND	14.1±7.6
NH_4^+	assimilation	2	1	ND	314±31
NH_4^+	assimilation	2	7	ND	ND
NH_4^+	assimilation	2	13	ND	ND
NH_4^+	oxidation to NO_2^-	2	1	ND	16.4±8.1

*Values reported are the mean ± standard error of triplicate measurements from independent bottles (i.e., three independent bottles per treatment per time point).

ND indicates that the rate was not determined. The second time interval of 13 hrs was not used for some samples because all of the ^{15}N spike had been exhausted (taken up) within the first 7 hrs of incubation (see text). The rates in the light were not determined for 1hour time points because they were measured before dawn.

Table 2: Net NO_2^- production rates. NO_2^- production was dominated by NO_3^- reduction by phytoplankton at depths of 60, 80, 160, and 200 m, and by NH_4^+ oxidation by nitrifying microbes at 120 m (NH_4^+ oxidation, see Fig. 8D and text for explanation). Rates were calculated from the change in concentration of NO_2^- between March 18 and March 24 at the onset of stratification, and are given on a per volume basis as well as on a per unit chl *a* basis. No values were calculated for 180 m because this depth was not sampled on March 18, so no change in NO_2^- concentration could be calculated.

Depth (m)	Light attenuation (% surface PAR)	Δ [NO_2^-] (nmol L^{-1})	chl *a* (μg L^{-1})	NO_2^- production rate (nmol L^{-1} day^{-1})	NO_2^- production rate (nmol μg chl a^{-1} day^{-1})
60	1	13	0.44	2.2	5.0
80	0.2	58	0.39	9.7	25
120	0.01	143	0.26	24	NA
160	0.0004	275	0.17	46	270
200	0.00002	345	0.19	58	290

NA indicates "not applicable" because the source of NO_2^- was NH_4^+ oxidizers rather than phytoplankton at this depth, so the rate was not normalized to chl *a*.

References

Allen, A. E., M. G. Booth, M. E. Frischer, P. G. Verity, J. P. Zehr, and S. Zani (2001), Diversity and detection of nitrate assimilation genes in marine bacteria, Applied and Environmental Microbiology 67, 5343-5348.

Allen, A. E., M. G. Booth, P. G. Verity, M. E. Frischer (2005) Influence of nitrate availability on the distribution and abundance of heterotrophic bacterial nitrate assimilation genes in the Barents Sea during summer, Aquatic Microbial Ecology 39, 247–255.

Al-Qutob, M., C. Hase, M. M. Tilzer, B. Lazar (2002), Phytoplankton drives nitrite dynamics in the Gulf of Aqaba, Red Sea. Marine Ecology Progress Series. 239, 233-239.

Altabet, M. A. 1988. Variations in nitrogen isotopic composition between sinking and suspended particles: implications for nitrogen cycling and particle transformation in the open ocean. Deep-Sea Research 35, 535-554.

Bronk, D. A., P. M. Gilbert, and B. B. Ward (1994), Nitrogen uptake, dissolved organic nitrogen release, and new production. Science 265, 1843-1846.

Cai, H. and N. Jiao (2008), Diversity and Abundance of Nitrate Assimilation Genes in the Northern South China Sea. Microb Ecol 56, 751–764 DOI 10.1007/s00248-008-9394-7.

Casciotti, K. L. (2009), Inverse kinetic isotope fractionation during bacterial nitrite oxidation. Geochimica et Cosmochimica Acta. 73, 2061-2076.

Casciotti, K. L., M. McIlvin, C. Buchwald (2010), Oxygen isotopic exchange and fractionation during bacterial ammonia oxidation. Limnology and Oceanography 55, 753–762.

Casciotti, K. L., D. M. Sigman, M. Galanter-Hastings, J. K. Bohlke, and A. Hilkert (2002), Measurement of the Oxygen Isotopic Composition of Nitrate in Seawater and Freshwater Using the Denitrifier Method. Analytical Chemistry, 74, 4905–4912.

Casciotti, K. L. and B. B. Ward (2006), Phylogenetic analysis of nitric oxide reductase gene homologues from aerobic ammonia-oxidizing bacteria. FEMS Microbiology Ecology 52, 197-205.

Casciotti, K. L., and B. B. Ward (2001), Dissimilatory Nitrite Reductase Genes from Autotrophic Ammonia-Oxidizing Bacteria Applied and Environmental Microbiology, 67, 2213-2221 DOI: 10.1128/AEM.67.5.2213-2221.2001.

Cohen Y. and M. Ottolenghi (2004), Gulf of Eilat Monitoring and Research Program -IET : Recommendations - Final Report. http://sviva.gov.il/Enviroment/Static/Binaries/Articals/final_report04_1.pdf

Collier, J. L., B. Brahamsha and B. Palenik (1999), The marine cyanobacterium Synechococcus sp. WH7805 requires urease (urea amiohydrolase, EC 3.5.1.5) to utilize urea as a nitrogen source: molecular-genetic and biochemical analysis of the enzyme. Microbiology 145, 447-459; DOI 10.1099/13500872-145-2-447.

Collos, Y. (1998), Nitrate, nitrite release and uptake, and new production estimates. Marine Ecology Progress Series 171, 293-301.

Cornell, S., A. Randell, and T. Jickells (1995), Atmospheric inputs of dissolved organic nitrogen to the oceans. Nature 376, 243 – 246.

D'Elia, C.F., P.A. Steudler, and N. Corwin (1977) Determination of total nitrogen in aqueous samples using persulfate digestion. Limnology and Oceanography 22, 760-764.

DeNiro M. J. and S. Epstein (1981), Influence of diet on the distribution of nitrogen isotopes in animals. Geochimica et Cosmochimica Acta 45, 341-351.

Dore, JE and DM Karl (1996a) Nitrite distributions and dynamics at Station ALOHA. Deep Sea Research Part II: Topical Studies in Oceanography 43, 385-402

Dore, JE and DM Karl (1996b) Nitrification in the Euphotic Zone as a Source for Nitrite, Nitrate, and Nitrous Oxide at Station ALOHA. Limnology and Oceanography 41, 1619-1628

Duce et al. (2008) Impacts of Atmospheric Anthropogenic Nitrogen on the Open Ocean. Science 320, 893 – 897.

Dugdale, R. C. and J. J. Goering (1967), Uptake of new and regenerated forms of nitrogen in primary productivity. Limnology and Oceanography 12, 196-206.

Dugdale, R. C. and F. P. Wilkerson. (1986), The Use of ^{15}N to Measure Nitrogen Uptake in Eutrophic Oceans; Experimental Considerations. Limnology and Oceanography 31, 673-689.

Eppley, RW, J. H. Sharp, E. H. Renger, M. J. Perry and W. G. Harrison (1977), Nitrogen assimilation by phytoplankton and other microorganisms in the surface waters of the central north Pacific Ocean. Marine Biology 39, 111-120.

Falkowski, P. G (1997), Evolution of the nitrogen cycle and its influence on the biological sequestration of CO_2 in the ocean. Nature 387, 272 – 275.

Fan, C., Glibert, P. M., Alexander, J., and Lomas, M. W. (2003), Characterization of urease activity in three marine phytoplankton species, Aureococcus anophagefferens, Prorocentrum minimum, and Thalassiosira weissflogii, Marine Biology 142, 949–958.

Foster, R. A., A. Paytan, and J. P. Zehr (2009), Seasonality of N_2 fixation and nifH gene diversity in the Gulf of Aqaba (Red Sea). Limnology and Oceanography 54, 219–233.

Francis, C. A., J. M. Beman and M. M. M. Kuypers. (2007), New processes and players in the nitrogen cycle: the microbial ecology of anaerobic and archaeal ammonia oxidation. The ISME Journal 1, 19-27.

Gilbert, P. M., F. Lipschultz, J. J. McCarthy, and M. A. Altabet (1982), Isotope dilution models of uptake and remineralization of ammonium by marine plankton. Limnology and Oceanography 27, 639-650.

Granger, J. and D. Sigman. (2009), Removal of nitrite with sulfamic acid for nitrate N and O isotope analysis with the denitrifier method. Rapid Communication in Mass Spectrometry 23, 3753–3762.

Granger, J., D. M. Sigman, J. A. Needoba and P. J. Harrison (2004), Coupled Nitrogen and Oxygen Isotope Fractionation of Nitrate during Assimilation by Cultures of Marine phytoplankton. Limnology and Oceanography 49, 1763-1773.

Granger, J, D. M. Sigman, M. M. Rohde, et al. (2010), N and O isotope effects during nitrate assimilation by unicellular prokaryotic and eukaryotic plankton cultures, Geochemica et Cosmochimica Acta. 74, 1030-1040.

Gruber, N., and J. L. Sarmiento (1997), Global Patterns of Marine Nitrogen Fixation and Denitrification, Global Biogeochem. Cycles 11, 235–266.

Guerrero, M. A., and R. D. Jones (1996), Photoinhibition of marine nitrifying bacteria. I. Wavelength-dependent response.Marine Ecology Progress Series 141, 183-192.

Hadas, O. and J. Erez (2004), IET Project No. C Nitrogen Fixation in the Gulf of Eilat In M. J. Atkinson, Y. Birk and H. Rosenthal [eds.], Evaluation of Fish Cages in the Gulf of Eilat, a technical report for the Israeli Ministries of Infrastructure Environment and Agriculture.

Hase, C., M. Al-Qutob, Z. Dubinsky, E. A. Ibrahim, B. Lazar, N. Stambler, M. M. Tilzer (2006), A system in balance? Implications of deep vertical mixing for the nitrogen budget in the

1031 northern Red Sea, including the Gulf of Aqaba (Eilat). Biogeosciences Discussions 3,
1032 383-408.
1033 Hollibaugh, J. T., and F. Azam (1983), Microbial degradation of dissolved proteins in seawater.
1034 Limnology and Oceanography 28, 1104–1116.
1035 Jackson, G. A. and P. M. Williams (1985), Importance of dissolved organic nitrogen and
1036 phosphorus to biological nutrient cycling. Deep Sea Research 32, 223-235.
1037 Kamennaya, N. A., M. Chernihovsky, and A. F. Post (2008), The cyanate utilization capacity of
1038 marine unicellular cyanobacteria. Limnology and Oceanography 53, 2485-2494.
1039 Karl, D., R. Letelier, L. Tupas, J. Dore1, J. Christian, and D. Hebel (1997), The role of nitrogen
1040 fixation in biogeochemical cycling in the subtropical North Pacific Ocean. Nature 388,
1041 533-538.
1042 Klotz, M. G, et al. (2006), Complete Genome Sequence of the Marine, Chemolithoautotrophic,
1043 Ammonia-Oxidizing Bacterium *Nitrosococcus oceani* ATCC 19707. Applied and
1044 Environmental Microbiology 72, 6299-6315.
1045 Knapp, A. N., DiFiore, P. J., Deutsch, C., Sigman, D. M. & Lipschultz, F. (2008) Nitrate isotopic
1046 composition between Bermuda and Puerto Rico: Implications for N_2 fixation in the
1047 Atlantic Ocean. Global Biogeochemical Cycles 22, GB3014,
1048 doi:10.1029/2007GB003107
1049 Koper, T., A. F. El-Sheikh, J. M. Norton, and M. G. Klotz (2004), Urease-encoding genes in
1050 ammonia-oxidizing bacteria. Applied and Environmental Microbiology, 70, 2342-2348.
1051 Leichter, J.J., A. Paytan, S. Wankel, K. Hanson, S. Miller and M.A. Altabet (2007), Nitrogen and
1052 oxygen isotopic signatures of subsurface nitrate: evidence of deep water nutrient sources
1053 to the Florida Keys reef tract. Limnology and Oceanography 52, 1258-1267.
1054 Lindell, D. and A. F. Post (1995), Ultraphytoplankton succession is triggered by deep winter
1055 mixing in the Gulf of Aqaba (Eilat), Red Sea. Limnology and Oceanography 40, 1130-
1056 1141.
1057 Lindell, D., E. Padan, and A. F. Post (1998), Regulation of ntcA Expression and Nitrite Uptake
1058 in the Marine Synechococcus sp. Strain WH 7803. Journal of Bacteriology 180, 1878-
1059 1886.
1060 Lomas, M. W. and P. M. Gilbert (1999), Temperature regulation of nitrate uptake: A novel
1061 hypothesis about nitrate uptake and reduction in cool-water diatoms. Limnology and
1062 Oceanography 44, 556-572.
1063 Lomas, M. W. and P. M. Gilbert (2000),Comparisons of nitrate uptake, storage and reduction in
1064 marine diatoms and dinoflagellates. Journal of Phycology 36, 903-913.
1065 Lomas, M. W. and F. Lipschultz (2006), Forming the primary nitrite maximum: Nitrifiers or
1066 phytoplankton? Limnology and Oceanography 51, 2453–2467.
1067 MacIsaac, J. J. and R. C. Dugdale (1972), Interactions of light and inorganic nitrogen in
1068 controlling nitrogen uptake in the sea. Deep Sea Research 19, 209-232.
1069 Mackey, K. R. M., R. G. Labiosa, M. Calhoun, J. Street, A. F. Post, A. Paytan (2007),
1070 Phosphorus availability, phytoplankton community dynamics, and taxon-specific
1071 phosphorus status in the Gulf of Aqaba, Red Sea. Limnology and Oceanography 52, 873–
1072 885.
1073 Mackey, K. R. M., T. Rivlin, A. Grossman, A. F. Post, and A. Paytan (2009), Picophytoplankton
1074 responses to changing nutrient and light regimes during a bloom. Marine Biology 156,
1075 1531-1546. DOI 10.1007/s00227-009-1185-2.

McCarthy, J. T. (1972), The Uptake of Urea by Natural Populations of Marine Phytoplankton. Limnology and Oceanography. 17, 738-748 .

McIlvin, M. R., and M. A. Altabet (2005), Chemical conversion of nitrate and nitrite to nitrous oxide for nitrogen and oxygen isotopic analysis in freshwater and seawater. Analytical Chemistry 77, 5589 -5595.

Meeder, E. KRM Mackey, A Paytan, Y Shaked, D Iluz, N Stambler, T Rivlin, AF Post 2, B Lazar. Nitrite dynamics in the open sea – A lesson from the northern Red Sea. In press Marine Ecology Progress Series.

Mingawa, M. and E. Wada. (1986), Nitrogen isotope ratios of red tide organisms in the East China Sea: A characterization of biological nitrogen fixation. Marine Chemistry 19, 245-259.

Montoya, J. P., C. M. Holl, J. P. Zehr, A. Hansen, T. A. Villareal & D. G. Capone (2004), High rates of N_2 fixation by unicellular diazotrophs in the oligotrophic Pacific Ocean. Nature 430:1027-1032 doi:10.1038/nature02824.

Moore, L. R., A. F. Post, G. Rocap and S. W. Chisholm. (2002), Utilization of Different Nitrogen Sources by the Marine Cyanobacteria Prochlorococcus and Synechococcus**.** Limnology and Oceanography, 47, 989-996.

Needoba, J. A. and P. J. Harrison. (2004), Influence of low light and a light: dark cycle on nitrate uptake, intracellular nitrate, and nitrogen isotope fractionation by marine phytoplankton. Journal of Phycology 40, 505-516.

Olson, R. (1981), Differential photoinhibition of marine nitrifying bacteria: A possible mechanism for the formation of the primary nitrite maximum. Journal of Marine Research 39, 227–238.

Opsahl, S. and R. Benner. (1997), Distribution and cycling of terrigenous dissolved organic matter in the ocean. Nature 386, 480–482.

Palenik, B., and F. M. Morel (1990), Amino acid utilization by marine phytoplankton—a novel mechanism. Limnology and Oceanography 35, 260-269.

Pantoja, S., D. J. Repeta, J. P. Sachs and D. M. Sigman (2002), Stable isotope constraints on the nitrogen cycle of the Mediterranean Sea water column. Deep-Sea Research I 49, 1609-1621.

Post, A. F., Z. Dedej, R.Gottlieb, H. Li, D. N. Thomas, M. Elabsawi, A. El-Naggar, M. El-Gharabawi, and U. Sommer. (2002), Spatial and temporal distribution of Trichodesmium spp. in the stratified Gulf of Aqaba, Red Sea. Marine Ecology Progress Series 239, 241–250.

Probyn T. A. and S. J. Painting. (1985), Nitrogen Uptake by Size-Fractionated Phytoplankton Populations in Antarctic Surface Waters. Limnology and Oceanography 30, 1327-1332.

Robertson, L. A., T. Dalsgaard, N.-P. Revsbeck, and J. G. Kuenen. (1995), Confirmation of aerobic denitrification in batch cultures, using gas chromatography and ^{15}N mass spectrometry. FEMS Microbiology Ecology 18, 113-120.

Sanudo-Wilhelmy, S. A. et al. (2001), Phosphorus limitation of nitrogen fixation by Trichodesmium in the central Atlantic Ocean. Nature 411, 66–69.

Schreiber, F. B. Loeffler, L. Polerecky, M. M. Kuypers, and D. de Beer (2009),http://www.nature.com/ismej/journal/v3/n11/full/ismej200955a.html - aff1#aff1 Mechanisms of transient nitric oxide and nitrous oxide production in a complex biofilm. The ISME Journal 3, 1301–1313 doi:10.1038/ismej.2009.55.

Sigman, D. M., Altabet, M. A., McCorkle, D. C., Francois, R. & Fischer, G. (2000) The ∂15N of nitrate in the Southern Ocean: Nitrogen cycling and circulation in the ocean interior. Journal of Geophysical Research 105 (C8), 19599-19614

Sigman, D. M., J. Granger, P. J. DiFiore, M. M. Lehmann, R. Ho, G. Cane, and A. van Geen (2005), Coupled nitrogen and oxygen isotope measurements of nitrate along the eastern North Pacific margin, Global Biogeochemical Cycles, 19, GB4022, doi:10.1029/2005GB002458.

Smayda, T. J. and B. Mitchell-Innes (1974), Dark survival of autotrophic, planktonic marine diatoms. Marine Biology 25, 195-202.

Solomon, C. M., J. L. Collier, G. M. Berg, P. M. Glibert (2010), Role of urea in microbial metabolism in aquatic systems: a biochemical and molecular review. Aquatic Microbial Ecology. 59, 67–88.

Starkenburg, S. R. (2006). Complete Genome Sequence of Nitrobacter hamburgensis X14 and Comparative Genomic Analysis of Species within the Genus Nitrobacter. Applied and Environmental Microbiology 74, 2852-2863.

Stepanauskas, R., H. Edling, and L. J. Tranvik (1999), Differential disolved organic nitrogen availability and bacterial aminopeptidase activity in limnic and marine waters. Microbial Ecology 38, 264–272.

Su, J.-J., B.-Y. Liu, and D.-Y. Liu. (2001), Comparison of aerobic denitrification under high oxygen atmosphere by *Thiosphaera pantotropha* ATCC 35512 and *Pseudomons stutzeri* SU2 newly isolated from the activated sludge of a piggery wastewater treatment system. Journal of Applied Microbiology 90, 457-462.

Tupas, L. M., I. Koike, D. M. Karl, and O. Holmhansen. (1994), Nitrogen metabolism by heterotrophic bacterial assemblages in Antarctic coastal waters. Polar Biol. 14, 195-204.

Wankel, S. D., Y. Chen, C. Kendall, A. F. Post, A. Paytan. (2009), Sources of aerosol nitrate to the Gulf of Aqaba: Evidence from [delta] ^{15}N and [delta] ^{18}O of nitrate and trace metal chemistry. Marine Chemistry: 120, 90-99.

Wankel, S. D., C. Kendall, J. T. Pennington, F. P. Chavez, and A. Paytan (2007), Nitrification in the euphotic zone as evidenced by nitrate dual isotopic composition: Observations from Monterey Bay, California, Global Biogeochemical Cycles, 21, GB2009,doi:10.1029/2006GB002723.

Wankel, S. D., C. Kendall, and A. Paytan. (2009), Using nitrate dual isotopic composition (δ15N and δ18O) as a tool for exploring sources and cycling of nitrate in an estuarine system: Elkhorn Slough, California. Journal of Geophysical Research, 114, G01011, doi:10.1029/2008JG000729.

Ward, B. B. (2005), Temporal variability in nitrification rates and related biogeochemical factors in Monterey Bay California, USA, Marine Ecology Progress Series. 292, 97–109.

Ward, B. B. (1985), Light and substrate concentration relationships with marine ammonium assimilation and oxidation rates. Marine Chemistry 16, 301-316.

Ward, B. B., and A. F. Carlucci. (1985) Marine ammonia-oxidizing and nitrite-oxidizing bacteria—serological diversity determined by immunofluorescence in culture and in the environment. Applied Environmental Microbiology 50, 194-201.

Ward, B. B., K. A. Kilpatrick, E. Renger, and R. W. Eppley. (1989), Biological nitrogen cycling in the nitracline. Limnology and Oceanography 34, 493-513.

Ward, B. B., R. J. Olson, and M. L. Perry. (1982), Microbial nitrification rates in the primary nitrite maximum off southern California. Deep Sea Research Part A. Oceanographic Research Papers 29, 247-255.

Wheeler, P. A. and D. L. Kirchman (1986), Utilization of inorganic and organic nitrogen by bacteria in marine systems. Limnology and Oceanography 31, 998-1009.

Wuchter C., B. Abbas, M. J. Coolen, L. Herfort,J. van Bleijswijk, P. Timmers, M. Strous, E. Teira, G. J. Herndl, J. J. Middelburg, S. Schouten, and J. S. Sinninghe Damsté (2006), Archaeal nitrification in the ocean, Proceedings of the National Academy of Science USA 103, 12317–12322.

Zafiriou, O, and M. True (1979), Nitrate photolysis in seawater by sunlight. Marine Chemistry 8, 9–32.

Zehr, J. P. and B. B. Ward (2002), Nitrogen Cycling in the Ocean: New Perspectives on Processes and Paradigms. Applied and Environmental Microbiology, 68, 1015-1024.

Zubkov, M. V., B. M. Fuchs, G. A. Tarran, P. H. Burkill, & R. Amann (2003), High Rate of uptake of organic nitrogen compounds by Prochlorococcus cyanobacteria as a key to their dominance in oligotrophic oceanic waters, Applied and Environmental Microbiology 69, 1299–1304 .

Figure Captions

Figure 1: The N cycle under oxic conditions, showing pathways and isotope effects of major N transformation processes (Casciotti 2009 and references therein). "ND" indicates that the isotope effect has not been determined.

Figure 2: Depth profiles of NO_3^- (shaded area), NO_2^- (black line), and chl *a* (green line) for January - December in (A) 2008 when the water column mixed down to the seafloor, and (B) 2003 when the mixing depth was ~400 m. During winter mixing NO_2^- accumulates and chl *a* is homogenously distributed in the mixed layer, regardless of the mixing depth. During summer stratification a PNM forms at or below the DCM. The euphotic depth is ~60 m in winter and ~100 m in summer.

Figure 3: Depth profiles collected at station A before (March 18) and during (March 24 and 25) the spring stratification event in 2008 showing (A) NO_3^-, NO_2^-, NH_4^+, and chl *a* concentrations. The red arrow shows the location of the NH_4^+ peak that was consumed during nitrification (see also Fig. 8D). (B) Cumulative N inventories of particulate N and DIN for depth transects collected at station A before (March 18) and during (March 24 and 25) the spring stratification event in 2008. (C) Total N inventories for depth transects collected at station A on March 24 and 25.

Figure 4: Cell abundances of *Synechococcus*, nanophytoplankton, picoeukaryotes, and non-photosynthetic microbes on March 24 (closed circles) and 25 (open circles). Note that different scales are used for each group.

Figure 5: Isotopic composition of N+N and PON on March 18, 24, and 25, showing (A) $\delta^{15}N_{N+N}$, (B) $\delta^{18}O_{N+N}$, and (C) $\delta^{15}N_{PON}$. Measured values for N+N are shown with open circles. Data with the correction applied to remove the NO_2^- signal as described in the text are shown by the grey line for $\delta^{15}N_{N+N}$ and $\delta^{18}O_{N+N}$.

Figure 6: Relationships between $\delta^{18}O_{N+N}$ and $\delta^{15}N_{N+N}$ for (A) March 18, (B) March 24, and (C) March 25. Data points are color coded as follows: euphotic zone (red), sub-euphotic zone (orange), upper PNM (green), and disphotic zone (black). The lines show the 1:1, 3:1 and 5:1 slopes anchored to $\delta^{15}N_{N+N}$ of 2.03 ‰ and $\delta^{18}O_{N+N}$ of 5.35 ‰ representing deep water in this region (600m, March 18th). Data with the correction applied to remove the NO_2^- signal (as described in the text) plot in a similar distribution, but are not shown in the graph for clarity.

Figure 7: N assimilation into particulate biomass in the ^{15}N tracer experiment for treatments spiked with A) NO_3^-, B) urea, C) NO_2^-, and D) NH_4. Error bars show standard error and are smaller than the symbols when not visible.

Figure 8: NO_3^- reduction to NO_2^- by phytoplankton is dependent on light and phytoplankton abundance (measured as chl *a*). (A) Light attenuation of photosynthetically active radiation (PAR) with depth on March 25 showing the depth where irradiance reached 1% surface PAR; designated by dotted arrows; (B) correlation of NO_3^- reduction rate with irradiance; (C) correlation of chl *a* with irradiance; (D) correlation of NO_3^- reduction with chl *a* with the effects

of light removed for both parameters (i.e. residuals are plotted). Analysis of residuals revealed that nitrification contributed substantially to NO_2^- formation at 120 m (open circle), where the data deviates from the best fit line (the best fit is based only on the closed circles).

Figure 9: Schematic diagram showing the principal regions of the NO_2^- profile as defined in this study. NA indicates that a process is not applicable at that depth.

Figure 1

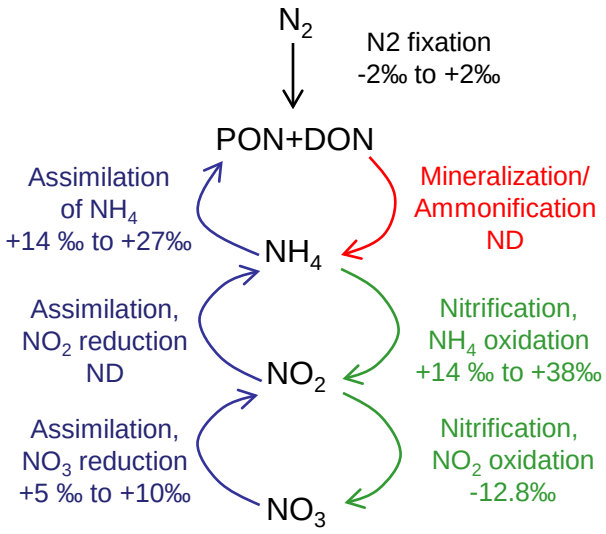
N_2
N2 fixation
-2‰ to +2‰
PON+DON
Assimilation of NH_4 +14 ‰ to +27‰
Mineralization/ Ammonification ND
NH_4
Assimilation, NO_2 reduction ND
Nitrification, NH_4 oxidation +14 ‰ to +38‰
NO_2
Assimilation, NO_3 reduction +5 ‰ to +10‰
Nitrification, NO_2 oxidation -12.8‰
NO_3

Figure 2

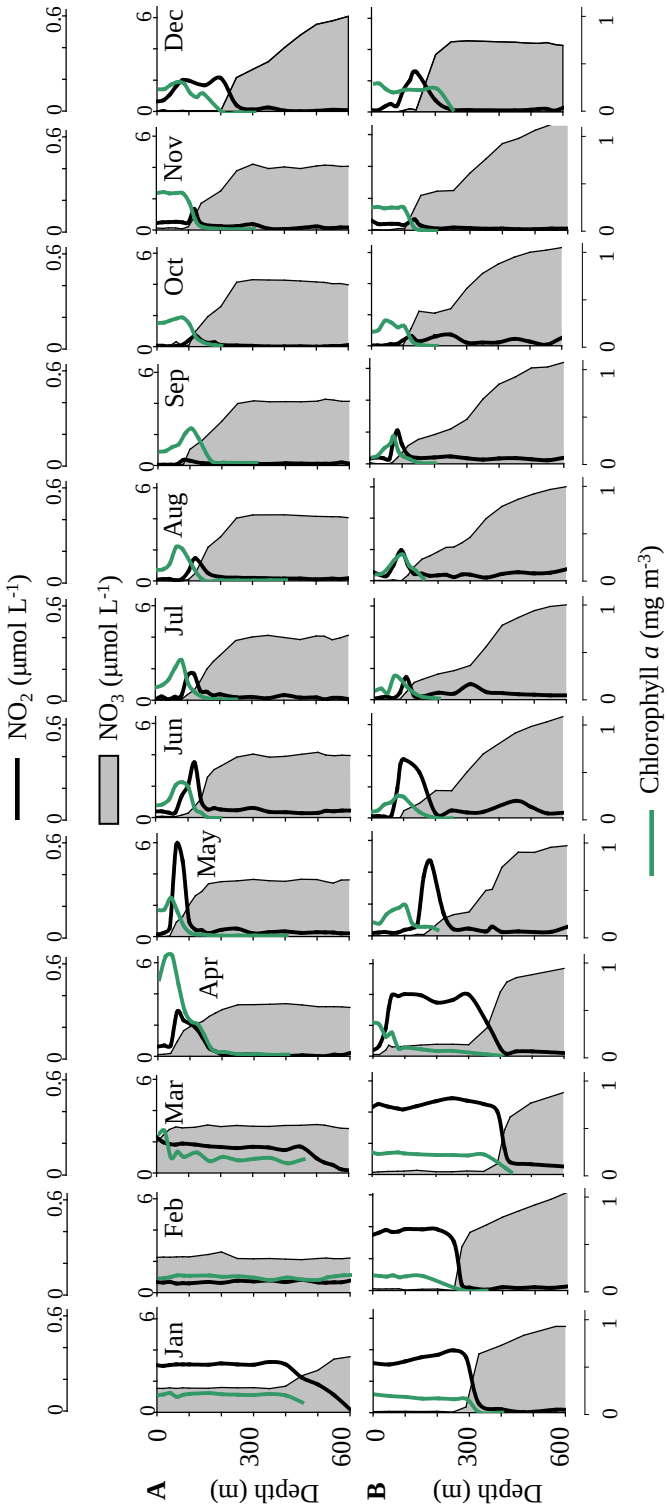
NO2 (µmol L-1)
NO3 (µmol L-1)
Chlorophyll a (mg m-3)
A
B
Depth (m)
Jan
Feb
Mar
Apr
May
Jun
Jul
Aug
Sep
Oct
Nov
Dec
0
300
600
0.6
6
1

Figure 3

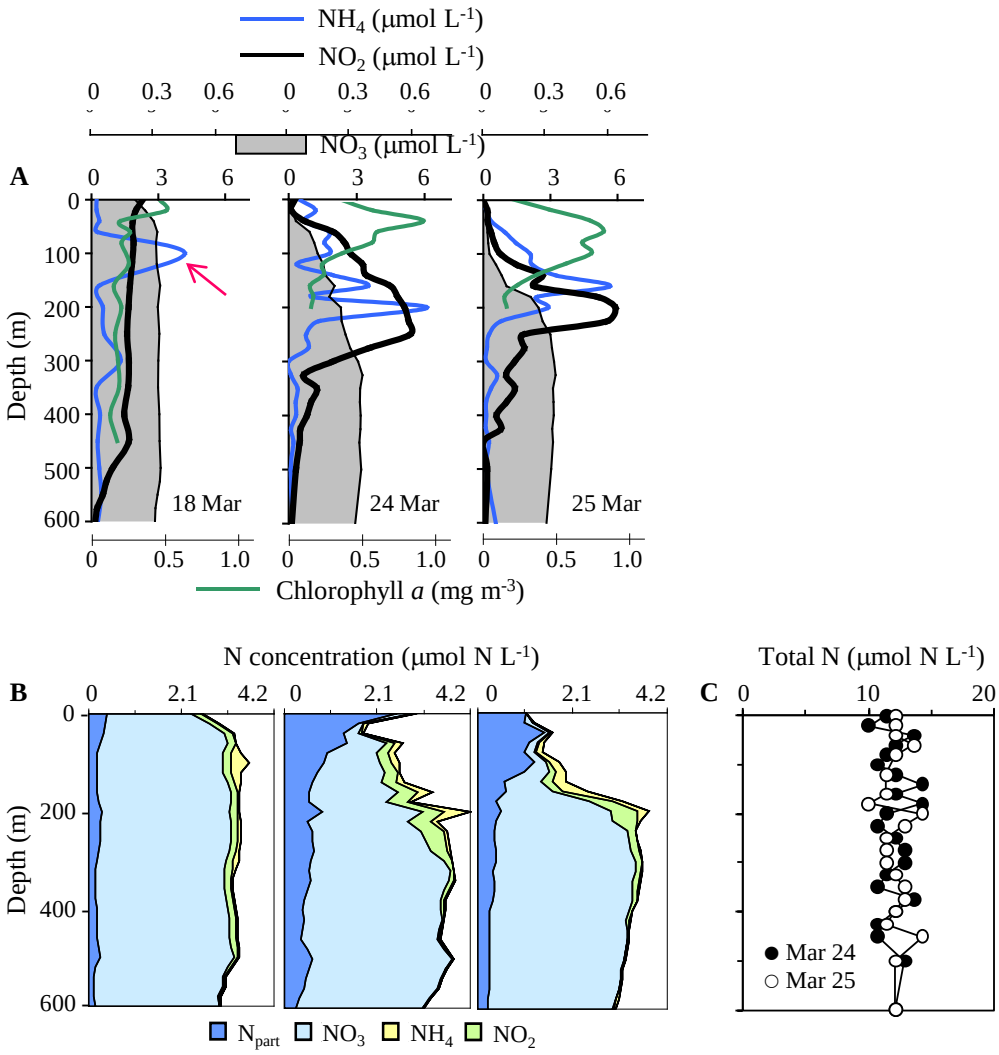
A
NH4 (µmol L-1)
NO2 (µmol L-1)
NO3 (µmol L-1)
Depth (m)
18 Mar
24 Mar
25 Mar
Chlorophyll a (mg m-3)
B
N concentration (µmol N L-1)
Npart
NO3
NH4
NO2
C
Total N (µmol N L-1)
Mar 24
Mar 25

Figure 4

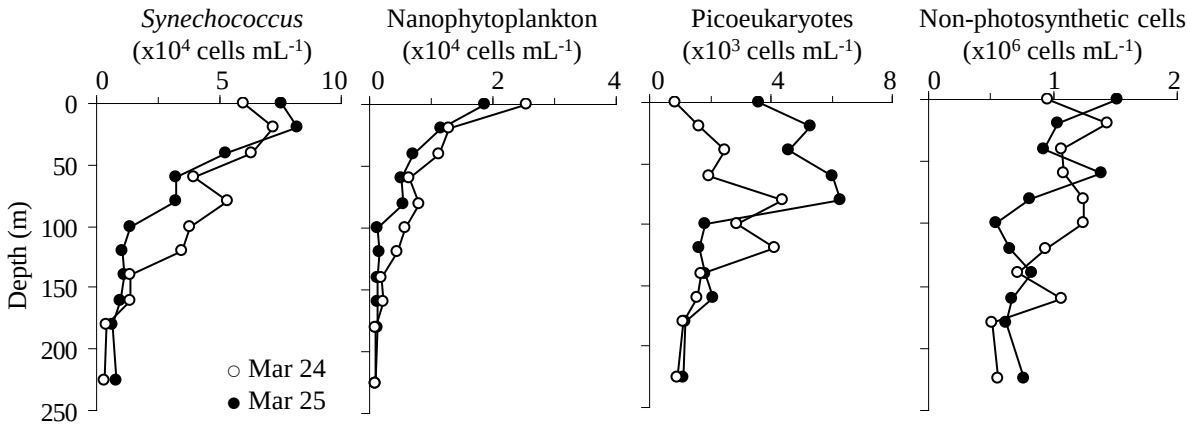
Synechococcus
(x10⁴ cells mL⁻¹)
Nanophytoplankton
(x10⁴ cells mL⁻¹)
Picoeukaryotes
(x10³ cells mL⁻¹)
Non-photosynthetic cells
(x10⁶ cells mL⁻¹)
Depth (m)
0
50
100
150
200
250
0
5
10
0
2
4
0
4
8
0
1
2
○ Mar 24
● Mar 25

Figure 5

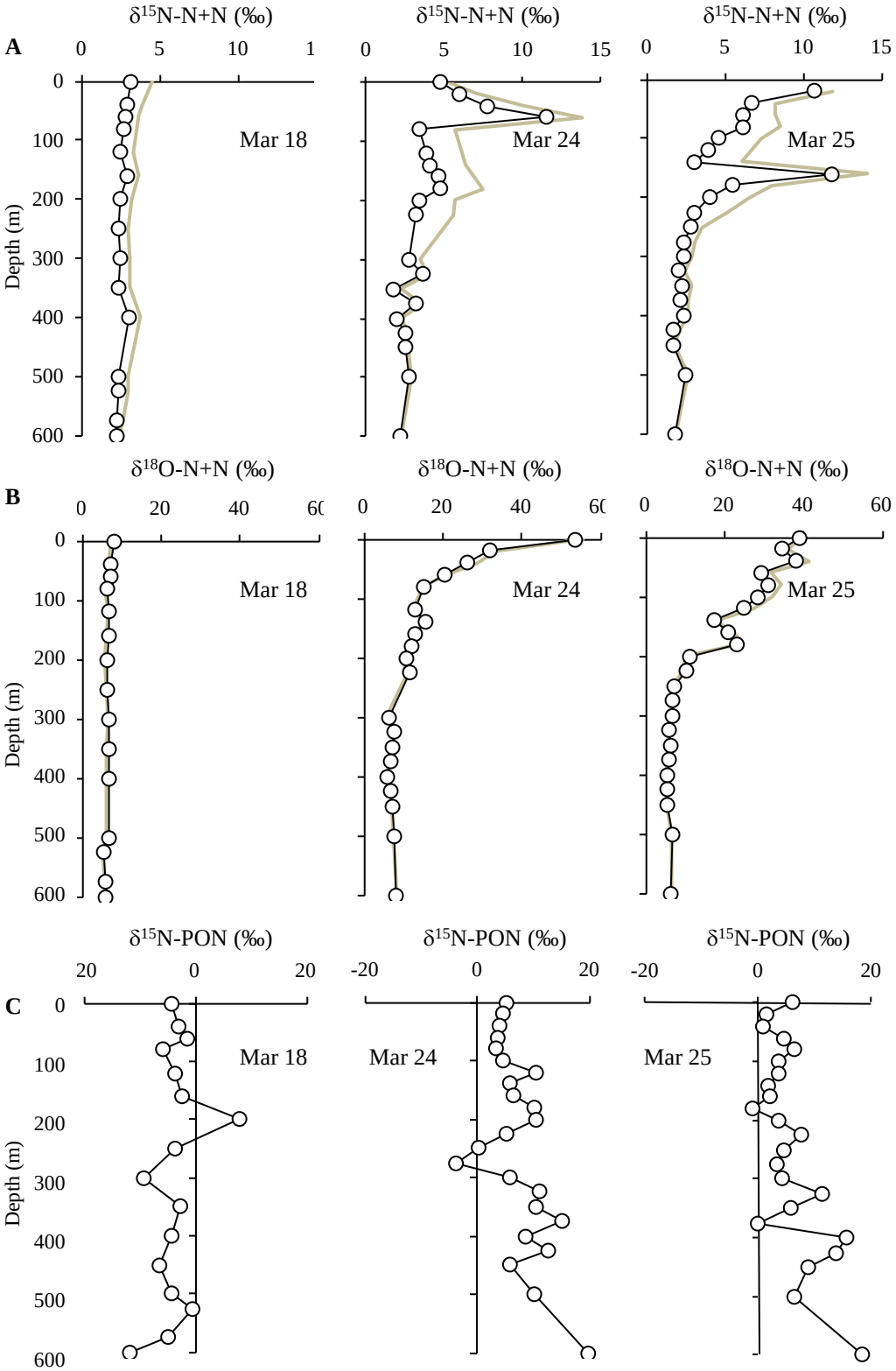
A
δ15N-N+N (‰)
Mar 18
Mar 24
Mar 25
Depth (m)
B
δ18O-N+N (‰)
Mar 18
Mar 24
Mar 25
Depth (m)
C
δ15N-PON (‰)
Mar 18
Mar 24
Mar 25
Depth (m)

Figure 6

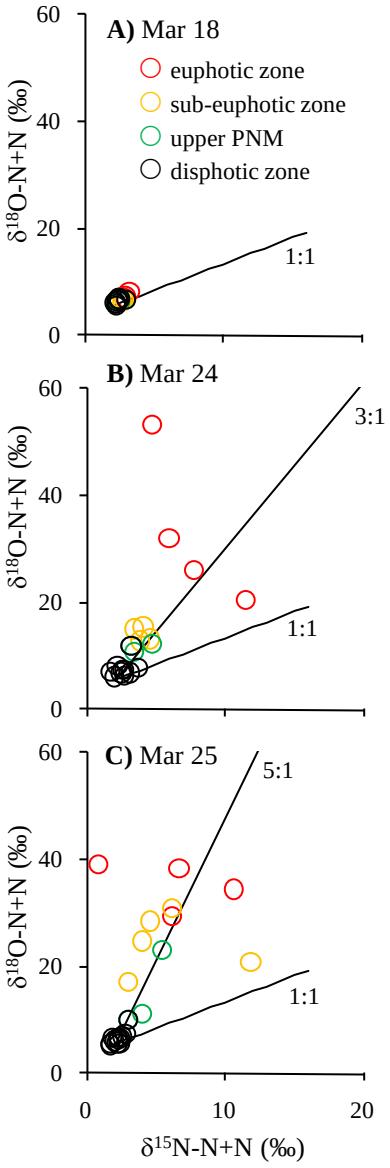
A) Mar 18
euphotic zone
sub-euphotic zone
upper PNM
disphotic zone
1:1
B) Mar 24
3:1
1:1
C) Mar 25
5:1
1:1
δ18O-N+N (‰)
δ15N-N+N (‰)
0
20
40
60
0
10
20

Figure 7

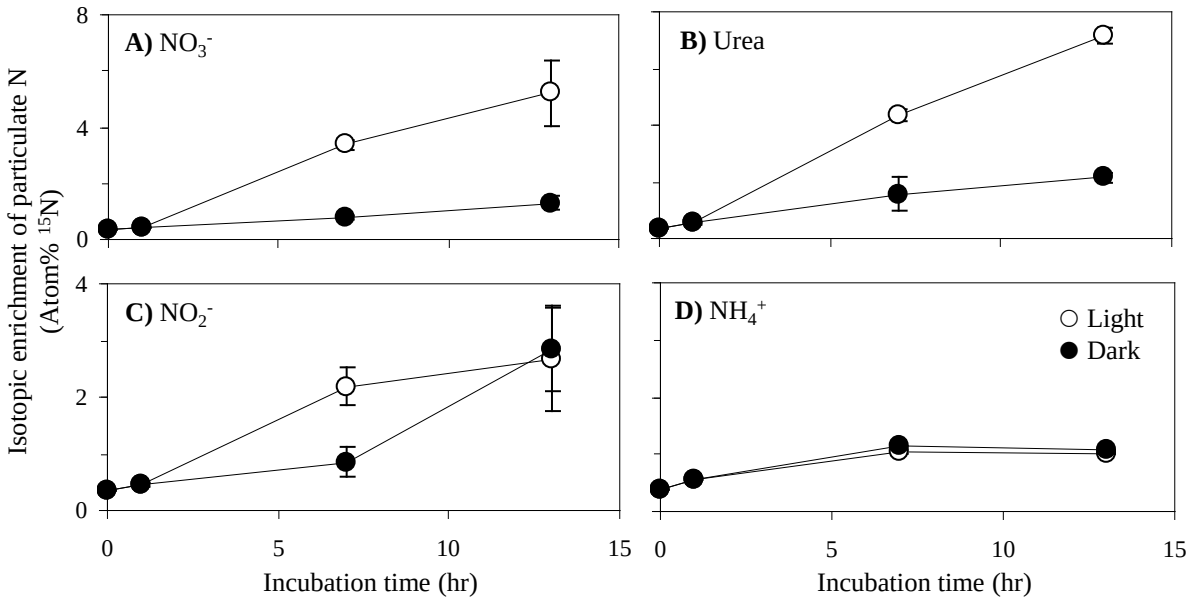
A) NO3-
B) Urea
C) NO2-
D) NH4+
Light
Dark
Isotopic enrichment of particulate N
(Atom% 15N)
Incubation time (hr)
Incubation time (hr)
0
4
8
0
2
4
0
5
10
15
0
5
10
15

Figure 8

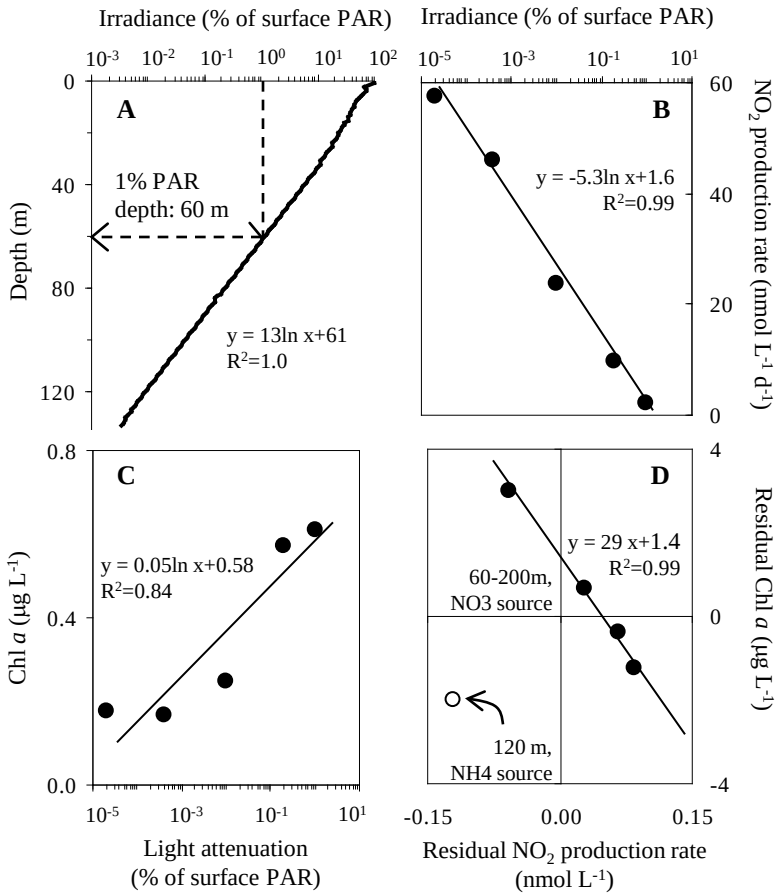
Irradiance (% of surface PAR)
Irradiance (% of surface PAR)
A
1% PAR
depth: 60 m
y = 13ln x+61
R²=1.0
Depth (m)
B
y = -5.3ln x+1.6
R²=0.99
NO2 production rate (nmol L-1 d-1)
C
y = 0.05ln x+0.58
R²=0.84
Chl a (µg L-1)
D
y = 29 x+1.4
R²=0.99
60-200m,
NO3 source
120 m,
NH4 source
Residual Chl a (µg L-1)
Light attenuation
(% of surface PAR)
Residual NO2 production rate
(nmol L-1)

Figure 9

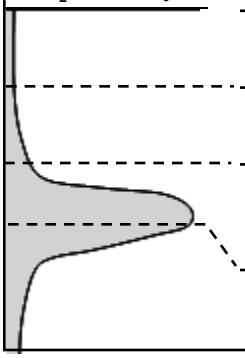

Water column region	PAR (%)	Assimilation	NO_3^- reduction by phytoplankton	Nitrification
Euphotic zone	>1	maximal	minimal	active; possibly limited to darkness (e.g. at night)
Sub-euphotic zone	0.001 – 1	minimal	maximal	active; possibly limited to darkness (depth dependent)
Upper PNM	<0.001	NA	maximal at stratification onset, minimal activity in ongoing stratification	uncoupled; NH_4^+ oxidation exceeds NO_2^- oxidation
Disphotic zone	<<0.001	NA	NA	coupled; NH_4^+ oxidation balances NO_2^- oxidation

NO_2^- inventory